suggested that cathepsin B is involved in proteolysis of FL-APP. Although it was initially demonstrated that cathepsin B has α-secretase-like activity through experiments with an artificial substrate that mimicked the α-secretase cleavage site (35), Hook *et al.* (14) showed that cathepsin B functioned as a β-secretase in the regulated secretory pathway against wild-type but not the Swedish mutation of APP. Moreover, it has been reported that cathepsin B has Aβ-degrading activity *in vivo* and *in vitro*, reducing the amount of amyloid plaques in aged AD model mice by lentivirus-mediated expression of cathepsin B (25). In the present study, cathepsin B seems to have no α- or β-secretase activity, and it may contribute to some Aβ degradation. However, cathepsin B is likely to be a multifunctional enzyme for APP metabolism; further studies are needed to establish its role in APP processing. First, for understanding the contribution of cathepsin B as β-secretase, it is important to estimate a ratio between Aβ present in the regulated secretory pathway and Aβ present in the constitutive secretory pathway in normal or AD brain. Second, from a different perspective, because treatment with CA-074Me results in acute inhibition of cathepsin B, there is no denying that a pharmacological approach with CA-074Me results in a different outcome than a genetic knockout experiment. As indicated above, cathepsin B-deficient mice exhibit no obvious phenotype, including the amounts of CTFs (25, 36); however, it has been suggested that cathepsin L compensates for the deficiency of cathepsin B. In this study, the treatment with E-64d, which is a broad cysteine protease inhibitor, caused accumulation of CTFα, CTFβ, and AICD. In cases in which CA-074Me loses the specificity of cathepsin B, cathepsin L also might be involved in degradation of CTFα, CTFβ, and AICD. Cathepsin B and L double-knockout mice are terminal during the second to fourth week of life and show neuronal loss (37). Although it has been reported that cathepsin B produces CTFβ in the regulated secretory pathway (14, 38, 39), our study clearly showed that cathepsin B degrades both CTFs and AICD. Since CTFs themselves are toxic (40) and AICD transgenic mice display age-dependent neurodegeneration (41), it may not be advisable to inhibit cathepsin B activity to treat AD, which may worsen rather than improve AD.

Protein phosphorylation, in particular, plays a significant role in a wide range of molecular and cellular biology. Reversible phosphorylation of proteins is an important regulatory mechanism that may influence conformational changes in the structure, altered localization, and enzymatic activity regulation. Phosphorylation of APP has been previously reported to induce a conformational change in the cytoplasmic region to alter interaction with Fe65, a neuronal-specific adaptor protein (42). The transfection of APP containing a Thr to Glu mutation (mimics phosphorylation) with Fe65 increases Aβ levels (42). Phosphorylation by stress-induced c-Jun N-terminal kinase (JNK) enhances proteolysis of pCTFs by γ-secretase (22). Although further investigation of the relationship between phosphorylation of APP and cathepsin B is required, we have provided indirect evidence that cathepsin B degrades CTFs at a constant rate without distinction for the phosphorylation state of the CTF (Fig. 7). Interestingly, inhibition of cathepsin B showed no significant difference in Aβ levels in our experimental paradigm (Supplemental Fig. S2). This result indicates that cathepsin B and γ-secretase share CTFs as a substrate but do not compete against each other. However, γ-secretase preferably hydrolyzed pCTFs over npCTFs (Fig. 7). Why inhibition of γ-secretase causes an increase in the ratio of the accumulation rate of pCTFs to the accumulation rate of CTFs and why inhibition of cathepsin B does not show this result are interesting puzzles still to be resolved. The significant decrease in the accumulation rate of CTFs in APP_{NL_TA}-H4 cells, as compared to that in APP_{NL}-H4 cells, when the γ-secretase inhibitor L-685,458 was administered confirms that APP phosphorylation regulates proteolysis of CTFs by γ-secretase. Cyclin-dependent kinase-5 (Cdk5), glycogen synthase kinase-3β (GSK-3β), and JNK are believed to phosphorylate APP at Thr668 (43), suggesting that inhibitors of these kinases would be effective drugs in the treatment of AD. Indeed, the GSK-3 inhibitor lithium chloride reduces Aβ levels (44). Kinase inhibitors, unlike γ-secretase inhibitors, would be expected to specifically block γ-cleavage of CTFs derived from APP without inhibition of γ-cleavage of other substrates (44). Furthermore, because these kinases also phosphorylate tau, which is a major component of neurofibrillary tangles, inhibition of these kinases decreases levels of hyperphosphorylated tau, preventing neurodegeneration and neuronal loss without Aβ reduction (45). In addition, based on our results and previous findings, serine/threonine phosphatases are also drug candidates. Protein phosphatase 2A (PP2A) is one of the most important phosphatases in the brain (46). PP2A activity decreases in AD brains (47), suggesting that Aβ is overproduced by activation of γ-secretase. This decreased PP2A activity also promotes phosphorylation of tau (47).

We propose the following model for roles of cathepsin B in APP processing. APP is metabolized by α- and β-secretase to generate CTFα and CTFβ, respectively. γ-Secretase and cathepsin B continuously hydrolyze CTFs; however, γ-secretase prefers the phosphorylated form of CTFs as substrates and then produces AICD from CTFs. pCTFs, npCTFs, and AICD are substrates for cathepsin B.

In summary, the present data demonstrate that cathepsin B contributes to the degradation of CTFs and AICD independently of α-, β-, and γ-secretases and that γ-secretase prefers pCTFs to npCTFs but cathepsin B does not. This study also suggests that reducing this phosphorylation may be a candidate for therapeutic intervention in AD. FJ

The authors thank Dr. Raphael Kopan (Washington University, St. Louis, MO, USA) for providing a plasmid (ΔEMV:

pCS2/Notch$^{\Delta E}$), Dr. Bart De Strooper (Katholieke Universiteit Leuven, Leuven, Belgium) for providing PS1 and PS2 double-knockout MEF *PS1*$^{-/-}$*PS2*$^{-/-}$ cells, and Drs. Taisuke Tomita and Takeshi Iwatsubo (The University of Tokyo, Tokyo, Japan) for providing mNotch$^{\Delta E}$-N2a cells. The authors also thank Dr. Kazumi Ishidoh (Tokushima Bunri University, Tokushima, Japan) for his valuable advice. This work was supported by the Regional Innovation Cluster Program (City Area Type; Central Saitama Area), the Shimabara Science Promotion Foundation, and a Grant-in-Aid for Scientific Research (C; 20590260) from the Japan Society for the Promotion of Science.

REFERENCES

1. Zheng, H., and Koo, E. H. (2006) The amyloid precursor protein: beyond amyloid. *Mol. Neurodegener.* **1,** 5
2. Marks, N., and Berg, M. J. (2008) Neurosecretases provide strategies to treat sporadic and familial Alzheimer disorders. *Neurochem. Int.* **52,** 184–215
3. Jacobsen, K. T., and Iverfeldt, K. (2009) Amyloid precursor protein and its homologues: a family of proteolysis-dependent receptors. *Cell. Mol. Life Sci.* **66,** 2299–2318
4. Panza, F., Solfrizzi, V., Frisardi, V., Capurso, C., D'Introno, A., Colacicco, A. M., Vendemiale, G., Capurso, A., and Imbimbo, B. P. (2009) Disease-modifying approach to the treatment of Alzheimer's disease: from α-secretase activators to γ-secretase inhibitors and modulators. *Drugs Aging* **26,** 537–555
5. Tomita, T. (2009) Secretase inhibitors and modulators for Alzheimer's disease treatment. *Expert Rev. Neurother.* **9,** 661–679
6. Doerfler, P., Shearman, M. S., and Perlmutter, R. M. (2001) Presenilin-dependent γ-secretase activity modulates thymocyte development. *Proc. Natl. Acad. Sci. U. S. A.* **98,** 9312–9317
7. Dovey, H. F., John, V., Anderson, J. P., Chen, L. Z., de Saint Andrieu, P., Fang, L. Y., Freedman, S. B., Folmer, B., Goldbach, E., Holsztynska, E. J., Hu, K. L., Johnson-Wood, K. L., Kennedy, S. L., Kholodenko, D., Knops, J. E., Latimer, L. H., Lee, M., Liao, Z., Lieberburg, I. M., Motter, R. N., Mutter, L. C., Nietz, J., Quinn, K. P., Sacchi, K. L., Seubert, P. A., Shopp, G. M., Thorsett, E. D., Tung, J. S., Wu, J., Yang, S., Yin, C. T., Schenk, D. B., May, P. C., Altstiel, L. D., Bender, M. H., Boggs, L. N., Britton, T. C., Clemens, J. C., Czilli, D. L., Dieckman-McGinty, D. K., Droste, J. J., Fuson, K. S., Gitter, B. D., Hyslop, P. A., Johnstone, E. M., Li, W.-Y., Little, S. P., Mabry, T. E., Miller, F. D., Ni, B., Nissen, J. S., Porter, W. J., Potts, B. D., Reel, J. K., Stephenson, D., Su, Y., Shipley, L. A., Whitesitt, C. A., Yin T., and Audia, J. E. (2001) Functional gamma-secretase inhibitors reduce beta-amyloid peptide levels in brain. *J. Neurochem.* **76,** 173–181
8. Gu, Y., Misonou, H., Sato, T., Dohmae, N., Takio, K., and Ihara, Y. (2001) Distinct intramembrane cleavage of the β-amyloid precursor protein family resembling γ-secretase-like cleavage of Notch. *J. Biol. Chem.* **276,** 35235–35238
9. Milano, J., McKay, J., Dagenais, C., Foster-Brown, L., Pognan, F., Gadient, R., Jacobs, R. T., Zacco, A., Greenberg, B., and Ciaccio, P. J. (2004) Modulation of notch processing by γ-secretase inhibitors causes intestinal goblet cell metaplasia and induction of genes known to specify gut secretory lineage differentiation. *Toxicol. Sci.* **82,** 341–358
10. Eisele, Y. S., Baumann, M., Klebl, B., Nordhammer, C., Jucker, M., and Kilger, E. (2007) Gleevec increases levels of the amyloid precursor protein intracellular domain and of the amyloid-β-degrading enzyme neprilysin. *Mol. Biol. Cell* **18,** 3591–3600
11. Vingtdeux, V., Hamdane, M., Bégard, S., Loyens, A., Delacourte, A., Beauvillain, J. C., Buée, L., Marambaud, P., and Sergeant, N. (2007) Intracellular pH regulates amyloid precursor protein intracellular domain accumulation. *Neurobiol. Dis.* **25,** 686–696
12. Hook, V. Y., Kindy, M., and Hook, G. (2008) Inhibitors of cathepsin B improve memory and reduce β-amyloid in transgenic Alzheimer disease mice expressing the wild-type, but not the Swedish mutant, β-secretase site of the amyloid precursor protein. *J. Biol. Chem.* **283,** 7745–7753
13. Van Acker, G. J., Saluja, A. K., Bhagat, L., Singh, V. P., Song, A. M., and Steer, M. L. (2002) Cathepsin B inhibition prevents trypsinogen activation and reduces pancreatitis severity. *Am. J. Physiol. Gastrointest. Liver Physiol.* **283,** G794–G800
14. Hook, V., Toneff, T., Bogyo, M., Greenbaum, D., Medzihradszky, K. F., Neveu, J., Lane, W., Hook, G., and Reisine, T. (2005) Inhibition of cathepsin B reduces β-amyloid production in regulated secretory vesicles of neuronal chromaffin cells: evidence for cathepsin B as a candidate β-secretase of Alzheimer's disease. *Biol. Chem.* **386,** 931–940
15. Ha, S. D., Martins, A., Khazaie, K., Han, J., Chan, B. M., and Kim, S. O. (2008) Cathepsin B is involved in the trafficking of TNF-α-containing vesicles to the plasma membrane in macrophages. *J. Immunol.* **181,** 690–697
16. Asai, M., Iwata, N., Tomita, T., Iwatsubo, T., Ishiura, S., Saido, T. C., and Maruyama, K. (2010) Efficient four-drug cocktail therapy targeting amyloid-β peptide for Alzheimer's disease. *J. Neurosci. Res.* **88,** 3588–3597
17. Asai, M., Iwata, N., Yoshikawa, A., Aizaki, Y., Ishiura, S., Saido, T. C., and Maruyama, K. (2007) Berberine alters the processing of Alzheimer's amyloid precursor protein to decrease Aβ secretion. *Biochem. Biophys. Res. Commun.* **352,** 498–502
18. Herreman, A., Serneels, L., Annaert, W., Collen, D., Schoonjans, L., and De Strooper, B. (2000) Total inactivation of γ-secretase activity in presenilin-deficient embryonic stem cells. *Nat. Cell Biol.* **2,** 461–462
19. De Duve, C., de Barsy, T., Poole, B., Trouet, A., Tulkens, P., and Van Hoof, F. (1974) Commentary. Lysosomotropic agents. *Biochem. Pharmacol.* **23,** 2495–2531
20. Gekle, M., Mildenberger, S., Freudinger, R., and Silbernagl, S. (1995) Endosomal alkalinization reduces J_{max} and K_m of albumin receptor-mediated endocytosis in OK cells. *Am. J. Physiol.* **268,** F899–F906
21. Yagishita, S., Morishima-Kawashima, M., Ishiura, S., and Ihara, Y. (2008) Aβ46 is processed to Aβ40 and Aβ43, but not to Aβ42, in the low density membrane domains. *J. Biol. Chem.* **283,** 733–738
22. Vingtdeux, V., Hamdane, M., Gompel, M., Bégard, S., Drobecq, H., Ghestem, A., Grosjean, M. E., Kostanjevecki, V., Grognet, P., Vanmechelen, E., Buée, L., Delacourte, A., and Sergeant, N. (2005) Phosphorylation of amyloid precursor carboxy-terminal fragments enhances their processing by a gamma-secretase-dependent mechanism. *Neurobiol. Dis.* **20,** 625–637
23. Nakanishi, H. (2003) Neuronal and microglial cathepsins in aging and age-related diseases. *Ageing Res. Rev.* **2,** 367–381
24. Guha, S., and Padh, H. (2008) Cathepsins: fundamental effectors of endolysosomal proteolysis. *Indian J. Biochem. Biophys.* **45,** 75–90
25. Mueller-Steiner, S., Zhou, Y., Arai, H., Roberson, E. D., Sun, B., Chen, J., Wang, X., Yu, G., Esposito, L., Mucke, L., and Gan, L. (2006) Antiamyloidogenic and neuroprotective functions of cathepsin B: implications for Alzheimer's disease. *Neuron* **51,** 703–714
26. Dice, J. F., and Terlecky, S. R. (1990) Targeting of cytosolic proteins to lysosomes for degradation. *Crit. Rev. Ther. Drug Carrier Syst.* **7,** 211–233
27. Cuervo, A. M. (2004) Autophagy: many paths to the same end. *Mol. Cell. Biochem.* **263,** 55–72
28. Kouchi, Z., Sorimachi, H., Suzuki, K., and Ishiura, S. (1999) Proteasome inhibitors induce the association of Alzheimer's amyloid precursor protein with Hsc73. *Biochem. Biophys. Res. Commun.* **254,** 804–810
29. Kinoshita, A., Fukumoto, H., Shah, T., Whelan, C. M., Irizarry, M. C., and Hyman, B. T. (2003) Demonstration by FRET of BACE interaction with the amyloid precursor protein at the cell surface and in early endosomes. *J. Cell Sci.* **116,** 3339–3346
30. Vetrivel, K. S., Cheng, H., Lin, W., Sakurai, T., Li, T., Nukina, N., Wong, P. C., Xu, H., and Thinakaran, G. (2004) Association of γ-secretase with lipid rafts in post-Golgi and endosome membranes. *J. Biol. Chem.* **279,** 44945–44954
31. Thinakaran, G., and Koo, E. H. (2008) Amyloid precursor protein trafficking, processing, and function. *J. Biol. Chem.* **283,** 29615–29619
32. Sun, B., Zhou, Y., Halabisky, B., Lo, I., Cho, S. H., Mueller-Steiner, S., Devidze, N., Wang, X., Grubb, A., and Gan, L. (2008)

Cystatin C-cathepsin B axis regulates amyloid beta levels and associated neuronal deficits in an animal model of Alzheimer's disease. *Neuron* **60,** 247–257
33. Von Rotz, R. C., Kohli, B. M., Bosset, J., Meier, M., Suzuki, T., Nitsch, R. M., and Konietzko, U. (2004) The APP intracellular domain forms nuclear multiprotein complexes and regulates the transcription of its own precursor. *J. Cell Sci.* **117,** 4435–4448
34. Pardossi-Piquard, R., Petit, A., Kawarai, T., Sunyach, C., Alves da Costa, C., Vincent, B., Ring, S., D'Adamio, L., Shen, J., Müller, U., St. George Hyslop, P., and Checler, F. (2005) Presenilin-dependent transcriptional control of the Aβ-degrading enzyme neprilysin by intracellular domains of βAPP and APLP. *Neuron* **46,** 541–554
35. Tagawa, K., Kunishita, T., Maruyama, K., Yoshikawa, K., Kominami, E., Tsuchiya, T., Suzuki, K., Tabira, T., Sugita, H., and Ishiura, S. (1991) Alzheimer's disease amyloid β-clipping enzyme (APP secretase): identification, purification, and characterization of the enzyme. *Biochem. Biophys. Res. Commun.* **177,** 377–387
36. Deussing, J., Roth, W., Saftig, P., Peters, C., Ploegh, H. L., and Villadangos, J. A. (1998) Cathepsins B and D are dispensable for major histocompatibility complex class II-mediated antigen presentation. *Proc. Natl. Acad. Sci. U. S. A.* **95,** 4516–4521
37. Felbor, U., Kessle, B., Mothes, W., Goebel, H. H., Ploegh, H. L., Bronson, R. T., and Olsen, B. R. (2002) Neuronal loss and brain atrophy in mice lacking cathepsins B and L. *Proc. Natl. Acad. Sci. U. S. A.* **99,** 7883–7888
38. Hook, V. Y., Kindy, M., Reinheckel, T., Peters, C., and Hook, G. (2009) Genetic cathepsin B deficiency reduces β-amyloid in transgenic mice expressing human wild-type amyloid precursor protein. *Biochem. Biophys. Res. Commun.* **386,** 284–288
39. Klein, D. M., Felsenstein, K. M., and Brenneman, D. E. (2009) Cathepsins B and L differentially regulate amyloid precursor protein processing. *J. Pharmacol. Exp. Ther.* **328,** 813–821
40. Kim, S. H., and Suh, Y. H. (1996) Neurotoxicity of a carboxyl-terminal fragment of the Alzheimer's amyloid precursor protein. *J. Neurochem.* **67,** 1172–1182
41. Ghosal, K., Vogt, D. L., Liang, M., Shen, Y., Lamb, B. T., and Pimplikar, S. W. (2009) Alzheimer's disease-like pathological features in transgenic mice expressing the APP intracellular domain. *Proc. Natl. Acad. Sci. U. S. A.* **106,** 18367–18372
42. Ando, K., Iijima, K. I., Elliott, J. I., Kirino, Y., and Suzuki, T. (2001) Phosphorylation-dependent regulation of the interaction of amyloid precursor protein with Fe65 affects the production of β-amyloid. *J. Biol. Chem.* **276,** 40353–40361
43. Suzuki, T., and Nakaya, T. (2008) Regulation of amyloid β-protein precursor by phosphorylation and protein interactions. *J. Biol. Chem.* **283,** 29633–29637
44. Rockenstein, E., Torrance, M., Adame, A., Mante, M., Bar-on, P., Rose, J. B., Crews, L., and Masliah, E. (2007) Neuroprotective effects of regulators of the glycogen synthase kinase-3β signaling pathway in a transgenic model of Alzheimer's disease are associated with reduced amyloid precursor protein phosphorylation. *J. Neurosci.* **27,** 1981–1991
45. Citron, M. (2010) Alzheimer's disease: strategies for disease modification. *Nat. Rev. Drug Discov.* **9,** 387–398
46. Janssens, V., and Goris, J. (2001) Protein phosphatase 2A: a highly regulated family of serine/threonine phosphatases implicated in cell growth and signaling. *Biochem. J.* **353,** 417–439
47. Liu, F., Grundke-Iqbal, I., Iqbal, K., and Gong, C. X. (2005) Contributions of protein phosphatases PP1, PP2A, PP2B and PP5 to the regulation of tau phosphorylation. *Eur. J. Neurosci.* **22,** 1942–1950

Received for publication February 1, 2011.
Accepted for publication June 23, 2011.

Journal of Neuroscience Research

Journal of Neuroscience Research 90:870–877 (2012)

Localization of Mature Neprilysin in Lipid Rafts

Kimihiko Sato,[1] Chiaki Tanabe,[2] Yoji Yonemura,[1] Haruhiko Watahiki,[1] Yimeng Zhao,[1] Sosuke Yagishita,[1] Maiko Ebina,[1] Satoshi Suo,[1] Eugene Futai,[1] Masayuki Murata,[1] and Shoichi Ishiura[1]*

[1]Department of Life Sciences, Graduate School of Arts and Sciences, The University of Tokyo, Tokyo, Japan

[2]Department of Neuroscience, School of Pharmacy, Iwate Medical University, Morioka, Japan

Alzheimer's disease (AD) is characterized by senile plaques caused by amyloid-β peptide (Aβ) accumulation. It has been reported that Aβ generation and accumulation occur in membrane microdomains, called *lipid rafts*, which are enriched in cholesterol and glycosphingolipids. Moreover, the ablation of cholesterol metabolism has been implicated in AD. Neprilysin (NEP), a neutral endopeptidase, is one of the major Aβ-degrading enzymes in the brain. Activation of NEP is a possible therapeutic target. However, it remains unknown whether the activity of NEP is regulated by its association with lipid rafts. Here we show that only the mature form of NEP, which has been glycosylated in the Golgi, exists in lipid rafts, where it is directly associated with phosphatidylserine. Moreover, the localization of NEP in lipid rafts is enhanced by its dimerization, as shown using the NEP E403C homodimerization mutant. However, the protease activities of the mature form of NEP, as assessed by in vitro peptide hydrolysis, did not differ between lipid rafts and nonlipid rafts. We conclude that cholesterol and other lipids regulate the localization of mature NEP to lipid rafts, where the substrate Aβ accumulates but does not modulate the protease activity of NEP.

Key words: Alzheimer's disease; neprilysin; lipid rafts

Alzheimer's disease (AD) is characterized by the formation of senile plaques, composed primarily of amyloid-β peptide (Aβ). Aβ deposition has been thought to cause neurofibrillary tangles, neuronal cell loss, vascular damage, and dementia (the amyloid hypothesis; Hardy and Higgins, 1992). It has recently been suggested that AD begins with hippocampal synaptic dysfunction caused by diffusible oligomeric assemblies of Aβ (Selkoe, 2002).

Aβ is produced from amyloid precursor protein (APP) by the action of β- and γ-secretases, although APP is usually cleaved within the Aβ sequence by α-secretase. Aβ is degraded by neprilysin (NEP; Iwata et al., 2001). NEP is a type II membrane metallopeptidase that is capable of degrading not only monomeric Aβ but also pathological oligomeric Aβ (Kanemitsu et al., 2003). It has been reported that NEP levels in the hippocampus and cortex decline with age (Iwata et al., 2002; Hellstrom-Lindahl et al., 2008). Thus, analysis of the mechanisms regulating NEP activity may provide valuable insights for new therapeutic targets.

Recently, there have been several reports on the activities of proteases being regulated by their localization to membrane microdomains, known as *lipid rafts*. Lipid rafts, which are enriched in cholesterol and glycosphingolipids, have been implicated in processes such as signal transduction, endocytosis, and cholesterol trafficking (Pike, 2004, 2006). Whereas α-secretase cleavage occurs in nonlipid rafts (Kojro et al., 2001; von Tresckow et al., 2004), Aβ generation occurs in lipid rafts (Wada et al., 2003). It has been reported that Aβ accumulation is initiated by its association with GM1 in lipid rafts (Matsuzaki et al., 2007) and that NEP is partially localized in lipid rafts (Angelisova et al., 1999; Riemann et al., 2001; Kawarabayashi et al., 2004). However, whether the activity of NEP is regulated by its localization in lipid rafts is unknown.

Here we show that localization of glycosylated mature NEP in lipid rafts is regulated by its association with cholesterol. Moreover, we show with the NEP E403C homodimerization mutant that this localization is enhanced by its dimerization. Furthermore, we investigated the protease activities of mature NEP by an in vitro peptide assay. Unexpectedly, they were comparable in lipid rafts and nonlipid rafts. These findings suggest

Additional Supporting Information may be found in the online version of this article.

K. Sato and C. Tanabe contributed equally to this work.

Contract grant sponsor: Ministry of Education, Science, Sports, Culture, and Technology of Japan.

*Correspondence to: Shoichi Ishiura, Department of Life Sciences, Graduate School of Arts and Sciences, The University of Tokyo, 3-8-1 Komaba, Meguro-ku, Tokyo 153-8902, Japan.
E-mail: cishiura@mail.ecc.u-tokyo.ac.jp

Received 2 June 2011; Revised 17 August 2011; Accepted 24 August 2011

Published online 20 December 2011 in Wiley Online Library (wileyonlinelibrary.com). DOI: 10.1002/jnr.22796

that cholesterol regulates the localization of mature NEP in lipid rafts, where the substrate Aβ accumulates but apparently does not modulate the protease activity of NEP.

MATERIALS AND METHODS

Vectors and Constructs

Human neprilysin, NEP WT, was inserted into the pcDNA3.1-3 × FLAG vector (Invitrogen, Carlsbad, CA), thereby fusing triplet tandem repeats of FLAG tag to its N-terminus. The expression product of this construct will be referred to as FLAG-NEP WT. NEP E584V, carrying a catalytically inactive mutant E584V, and NEP E403C, carrying a homodimerization mutant, were subcloned into the pcDNA3.1-3 × FLAG vector, yielding FLAG-NEP E584V and FLAG-NEP E403C, respectively.

Antibodies

The following antibodies were purchased: anti-FLAG M2 (Sigma, St. Louis, MO); antiflotillin-1 and anticalnexin (BD Transduction Laboratories, Lexington, KY); anti-monoclonal NEP (Leica Microsystems); and HRP-conjugated anti-mouse IgG (Cell Signaling Technology, Beverly, MA).

Cell Culture and Transfection

HEK293 cells were cultured in DMEM (Sigma) supplemented with 10% fetal bovine serum (Sigma). They were maintained at 37°C in an atmosphere containing 5% CO_2 in a tissue culture incubator. DNA transfection was performed by lipofection with FuGENE 6 Transfection Reagent (Roche, Indianapolis, IN) when cells were 50% confluent. Then, 24 hr later, cells were harvested or used in assays.

Isolation of the Membrane Fraction

Cells were dissolved in TBS (0.1 M Tris-HCl, pH 8.0, 150 mM NaCl) containing Complete, EDTA-free protease inhibitor (Roche) and 0.7 μg/ml pepstatin A (Sigma) and disrupted by passage 20 times through a 21-G needle. The cell sample was then centrifuged (2,000 rpm, 2 min, 4°C). The resulting supernatant was then centrifuged again (49,000 rpm, 30 min, 4°C; Optima MAX-E ultracentrifuge; Beckman Coulter). The pellet formed was dissolved in TBS containing Complete, EDTA-free protease inhibitors, 0.7 μg/ml pepstatin A, and 1% Triton X-100; incubated on ice for 1 hr; and ultracentrifuged again. The resulting supernatant will be referred to as the *membrane fraction*.

Enzymatic Deglycosylation

The membrane fraction was solubilized with 1% Triton X-100 and then deglycosylated through treatment with the following: 1) endoglycosidase H (endo H; BioLabs), according to the manufacturer's instructions, and 2) 1 U N-glycosidase F (Endo F; Roche) per 45 μg of protein. The membrane fraction was denatured by boiling for 3 min in 1% SDS and 2-mercaptoethanol (ME), suspended in a reaction buffer (50 mM EDTA, 1% 2-ME, 0.5% Triton X-100, 0.1% SDS, 1 U N-glycosidase F) containing Complete, EDTA-free protease inhibitors and 0.7 μg/ml pepstatin A and incubated at 37°C overnight.

Isolation of Lipid Rafts by Sucrose Density Gradient Centrifugation

Cells were lysed on ice in MBS buffer (25 mM MES, pH 6.5, 150 mM NaCl) containing 1% Triton X-100, Complete, EDTA-free protease inhibitors, and 0.7 μg/ml pepstatin A. Cell disruption was achieved by passing the lysate 10 times through a 21-G needle and then 20 times through a 27-G needle. The lysate was incubated at 4°C for 30 min, and an equal amount of 80% sucrose was then added to it. The sample and sucrose buffer, containing 5–40% sucrose, were sequentially loaded to the bottom of a tube and then centrifuged (36,000 rpm, 18 hr, 4°C; CP 70 WX ultracentrifuge; Hitachi). Fractions were collected from the top to the bottom. Equal volumes of these samples were analyzed by Western blotting.

Methyl-β-Cyclodextrin Treatment

HEK293 cells overexpressing FLAG NEP-WT were washed with PBS, treated with 10 mM methyl-β-cyclodextrin (MβCD; Trappsol) for 20 min in a CO_2 incubator at 37°C, and collected. Lipid rafts fractions were treated with 50 mM MβCD on ice for 1 hr, dissolved in a double volume of TBS containing Complete, EDTA-free protease inhibitors and 0.7 μg/ml pepstatin A, and centrifuged (49,000 rpm, 1 hr, 4°C). The supernatants were removed and the pellets dissolved in TBS.

Western Blotting

Equal amounts of protein samples were separated by SDS-PAGE or Blue Native-PAGE and transferred to Immobilon-P PVDF membranes (Millipore, Billerica, MA). In the case of Blue Native-PAGE, the membranes were washed and destained using methanol. The membranes were soaked in PBS containing 5% nonfat dried milk and 0.05% Tween for 1 hr and then incubated overnight at 4°C with primary antibodies diluted in PBS containing 0.05% Tween, 0.1% BSA, and 1 mM NaN_3. After washing, the membranes were incubated with HRP-conjugated secondary antibody for 1 hr. Antigen–antibody complexes were detected by enhanced chemiluminescence using a LAS-3000 Luminescent Image Analyzer (Fujifilm). Signals were quantified in MultiGauge software (version 2.3; Fujifilm).

Assay of NEP-Dependent Neutral Endopeptidase Activity

NEP activity was measured in vitro by incubation at 37°C for 1 hr in 100 mM MES (pH 6.8) containing Complete, EDTA-free protease inhibitors, 10 μM Z-Leu-Leu-Leu-H, and as a substrate 50 μM Z-Ala-Ala-Leu-*p*-nitroanilide (ZALL-*p*-NA; Peptide Institute), in the presence or absence of 10 μM thiorphan, a specific inhibitor of NEP.

Interaction of NEP With Various Lipids

Lipid-spotted membrane (P-6002; Echelon Biosciences) was treated with TBS containing 1% skim milk and gently

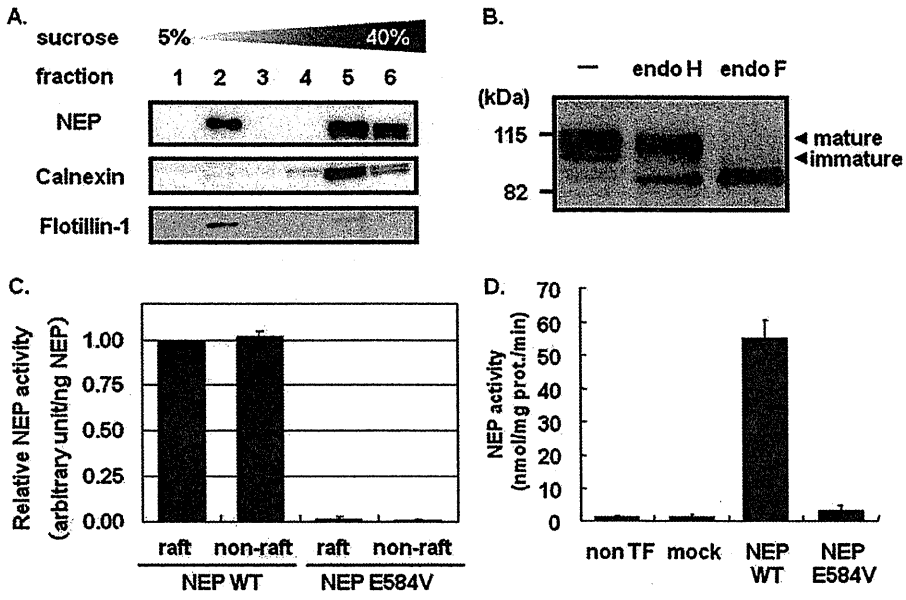

Fig. 1. NEP localization and activity in lipid rafts. **A:** Western blot analysis of lipid rafts fractionated from HEK293 cells overexpressing FLAG-NEP WT by a sucrose density-gradient centrifugation method. An anti-FLAG antibody was used to detect NEP. Lipid rafts were detected using an antibody raised against the raft marker flotillin-1. Nonlipid rafts (fraction 5) were detected using an antibody raised against the nonraft marker calnexin. **B:** Deglycosylation of the membrane fraction prepared from HEK293 cells overexpressing FLAG-NEP WT. The membrane fraction was treated with endoglycosidase H (endo H) and endoglycosidase F (endo F) or left untreated as a control (–), and then analyzed by Western blotting with an anti-FLAG antibody. **C:** Comparison of the specific enzymatic activity of the mature form NEP in lipid rafts (fraction 2) and nonlipid rafts (fraction 5), as assessed by *p*-NA peptide assay. Values represent the mean ± SD of three experiments. **D:** Neprilysin-dependent neutral endopeptidase activity in membrane fractions prepared from nontransfected HEK293 cells (non-TF) and cells transfected with vector (mock), FLAG-NEP WT (NEP WT) or the catalytically inactive mutant FLAG-NEP E584V. Values represent the mean ± SD of three experiments.

agitated for 1 hr at room temperature. SH-SY5Y neuronal cells were fractionated by sucrose density gradient centrifugation as shown previously, and each fraction was added to an equal volume of TBS containing protease inhibitor cocktail. After centrifugation at 49,000 rpm for 1 hr, the precipitate was dissolved in TBS containing protease inhibitor cocktail and incubated with the P-6002 membrane for 1 hr at room temperature. After incubation, the membrane was washed with TBS containing 0.1% Tween three times and incubated with anti-NEP monoclonal antibody diluted 1:2,000 for 1 hr at room temperature. The bound NEP was detected with an ECL advance kit (GE Healthcare, Amersham, United Kingdom).

RESULTS

Localization and Peptidase Activity of NEP in Lipid Rafts

To evaluate the peptidase activity of NEP in lipid rafts, we fractionated lipid rafts by sucrose density gradient centrifugation. We analyzed the localization of membrane-bound NEP extracted from HEK293 cells overexpressing FLAG-NEP WT. A raft marker, flotillin-1, was detected in fraction 2 and a nonraft marker, calnexin, in fractions 5 and 6 (Fig. 1A). FLAG-NEP was detected as a single band in fraction 2 and doublet bands in fractions 5 and 6. To distinguish these doublet bands, we deglycosylated the membrane fraction by treating it with endoglycosidase H (endo H) and endoglycosidase F (endo F; Fig. 1B). Although the upper band, the mature form, was resistant to endo H treatment, the lower band was deglycosylated by endo H. We will refer to the latter as the *immature form* of NEP. Resistance to endo H is acquired on transport of the protein to the Golgi apparatus, and this glycosylation is important for the catalytic activity of NEP (Lafrance et al., 1994). We compared the specific enzymatic activity of the mature form of NEP in lipid rafts (fraction 2) and nonlipid rafts (fraction 5); the contents of mature NEP were equalized by densitometric measurement of mature NEP levels after immunoblotting with an anti-FLAG antibody. The NEP activities of fractions 2 and 5, as assessed by *p*-NA peptide assay, were comparable (Fig. 1C). In this assay, catalytically inactive NEP E584V was used as a negative control (Fig. 1D).

Localization of NEP in Lipid Rafts Is Dependent on Cholesterol

Only mature NEP was detected in lipid rafts (Fig. 1A). We thus hypothesized that cholesterol in lipid rafts regulated the localization of mature NEP. To test this, we depleted HEK293 cells overexpressing FLAG-NEP

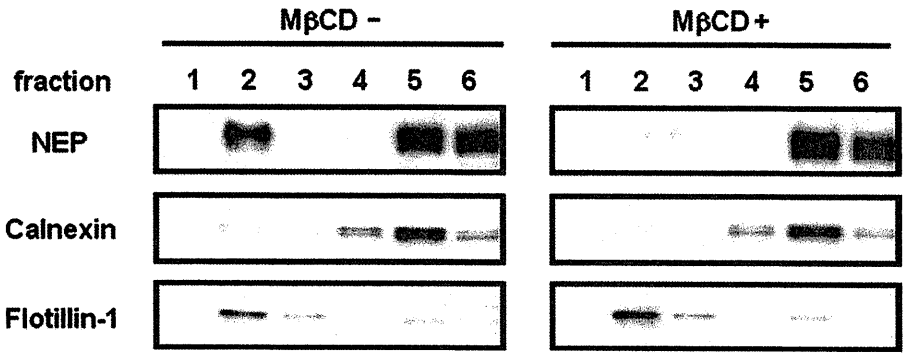

Fig. 2. Delocalization of NEP from lipid rafts in cells treated with MβCD. HEK293 cells overexpressing FLAG-NEP WT were treated with methyl-β-cyclodextrin (MβCD; +) or left untreated (–), and lipid rafts were fractionated as described in Materials and Methods.

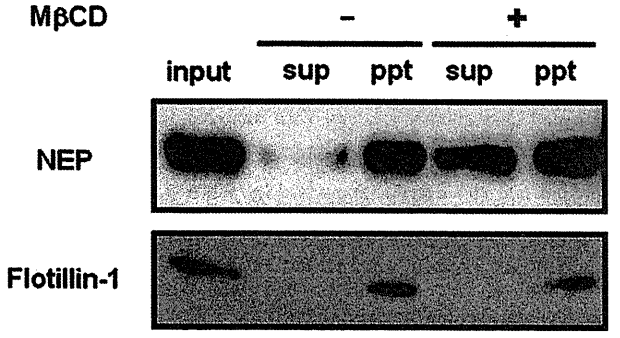

Fig. 3. Delocalization of NEP from fractionated lipid rafts after MβCD treatment. The lipid raft fraction, isolated from HEK293 cells overexpressing FLAG-NEP WT, was treated with (+) MβCD or left untreated (–) and separated into a supernatant (Sup) and a pellet (Ppt) by ultracentrifugation. The distribution of NEP was determined by Western blotting with an anti-FLAG antibody.

WT of cholesterol by treating them with 10 mM methyl-β-cyclodextrin (MβCD) for 20 min, and then fractionated the lipid rafts. More than 50% of cholesterol can be depleted from HEK293 cells by this treatment (Kojro et al., 2001). NEP became delocalized from lipid rafts following MβCD treatment, although flotillin-1 remained associated with them (Fig. 2).

We confirmed that the in vitro depletion of cholesterol from the lipid rafts fraction caused the delocalization of NEP from lipid rafts. We treated the fractionated lipid rafts with 50 mM MβCD for 1 hr at 4°C and separated them into supernatants and pellets by ultracentrifugation (Fig. 3). NEP and flotillin-1, associated with lipid rafts, were detected, as expected, in the pellets formed from lipid rafts not treated with MβCD. However, some of the NEP associated with lipid rafts was detected in supernatants prepared from lipid rafts treated with MβCD treatment. Flotillin-1 remained exclusively in the pellets, suggesting that flotillin-1 was not associated with choresterol.

Localization of NEP in Lipid Rafts Is Enhanced by Its Dimerization

To understand better the mechanism of NEP localization in lipid rafts, we investigated whether NEP dimerization facilitated the assembly of the enzyme in lipid rafts. We lysed HEK293 cells overexpressing FLAG-NEP WT in buffers containing different detergents and then analyzed NEP protein complexes by Blue Native-PAGE. Although NEP complexes were dissociated by NP-40 and Triton X-100, the 300-kDa complexes were resistant to treatment with DDM and digitonin (Fig. 4A). Next, we investigated the effect of dimerization on the localization of NEP in lipid rafts. It has been reported that rabbit NEP carrying an E403C mutation forms a covalent homodimer (Hoang et al., 1997). We introduced this mutation into human NEP and assessed its effect on the localization of NEP in lipid rafts. FLAG-NEP WT and FLAG-NEP E403C were detected as single 120-kDa bands after their separation by SDS-PAGE under reducing conditions (Fig. 4B). A 250-kDa FLAG-NEP E403C homodimer was detected under nonreducing conditions (Fig. 4B). These results indicate that, as in rabbit NEP, the E403C mutation caused human NEP to form of a covalent homodimer. Interestingly, although NEP WT complexes (Fig. 4A,C) were not resistant to Triton X-100, the NEP E403C mutant was resistant to Triton X-100 and formed a disulfide-bonded complex the same size as the NEP WT complex. Although we cannot exclude the possibility that the complex includes other proteins, the 300-kDa complex (Fig. 4A,C) appears to represent a covalent NEP homodimer.

Next, we compared the localization of mature forms of NEP WT and NEP E403C in lipid rafts. The ratio of the amount of mature NEP localized in lipid rafts to the total amount of mature NEP was 1.3 times higher in HEK293 cells overexpressing homodimeric mutant NEP E403C (47.7%) than in those expressing NEP WT (35.7%; Fig. 4D). These results demonstrate that the localization of NEP in lipid rafts was enhanced by its dimerization.

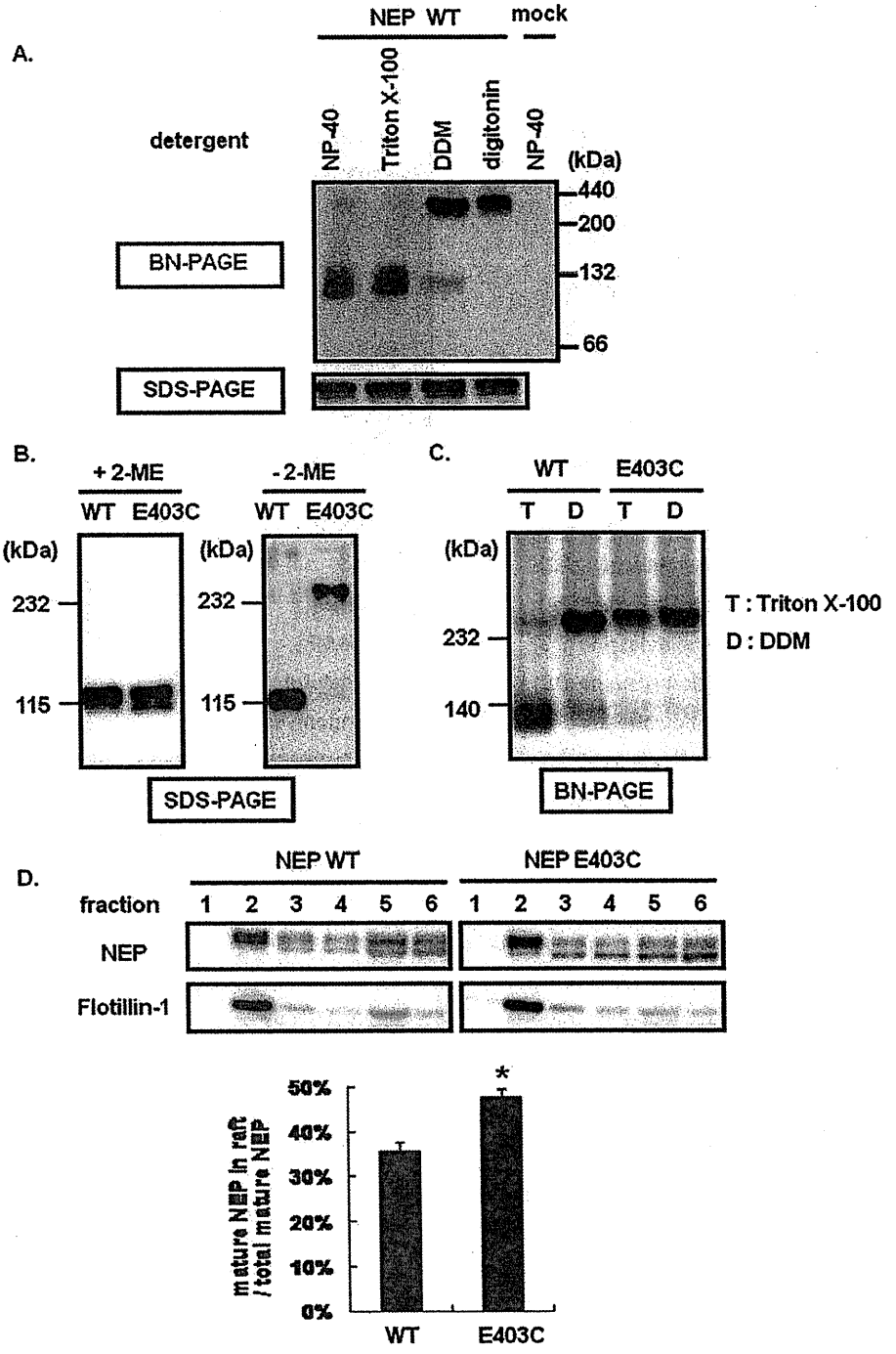

Fig. 4. Dimerization and localization of human NEP E403C in lipid rafts. **A:** Membrane fractions prepared from HEK293 cells overexpressing FLAG-NEP WT (NEP WT) or vector (mock) were dissolved in buffer containing detergents, such as NP-40, Triton X-100, DDM, and digitonin (all at a concentration of 1%). NEP complexes were analyzed by Blue Native-PAGE (BN-PAGE) or SDS-PAGE, followed by Western blotting with an anti-FLAG antibody. **B:** Membrane fractions obtained from HEK293 cells overexpressing FLAG-NEP WT (WT) or FLAG-NEP E403C (E403C) were analyzed by SDS-PAGE, performed with (**left**) or without (**right**) 2-ME. **C:** Membrane fractions obtained from HEK293 cells overexpressing FLAG-NEP WT (WT) or FLAG-NEP E403C (E403C) were dissolved in buffer containing 1% Triton X-100 (T) or 1% of DDM (D). The resulting lysates were analyzed by Blue Native-PAGE (BN-PAGE) and Western blotting with an anti-FLAG antibody. **D:** Effect of the E403C mutation on the distribution of NEP in lipid rafts. Lipid rafts from HEK293 cells overexpressing FLAG-NEP WT (NEP WT) or FLAG-NEP E403C (NEP E403C) were fractionated by sucrose density-gradient centrifugation and analyzed by Western blotting with an anti-FLAG antibody. The ratio of the amount of mature NEP localized in lipid rafts to the total amount of mature NEP was determined by densitometric measurement of protein bands corresponding to the mature form of NEP. Values represent the mean ± SD of three experiments. Statistical analysis was performed using a two-tailed Student's *t*-test. $*P < 0.05$ was considered to indicate statistical significance (bottom graph).

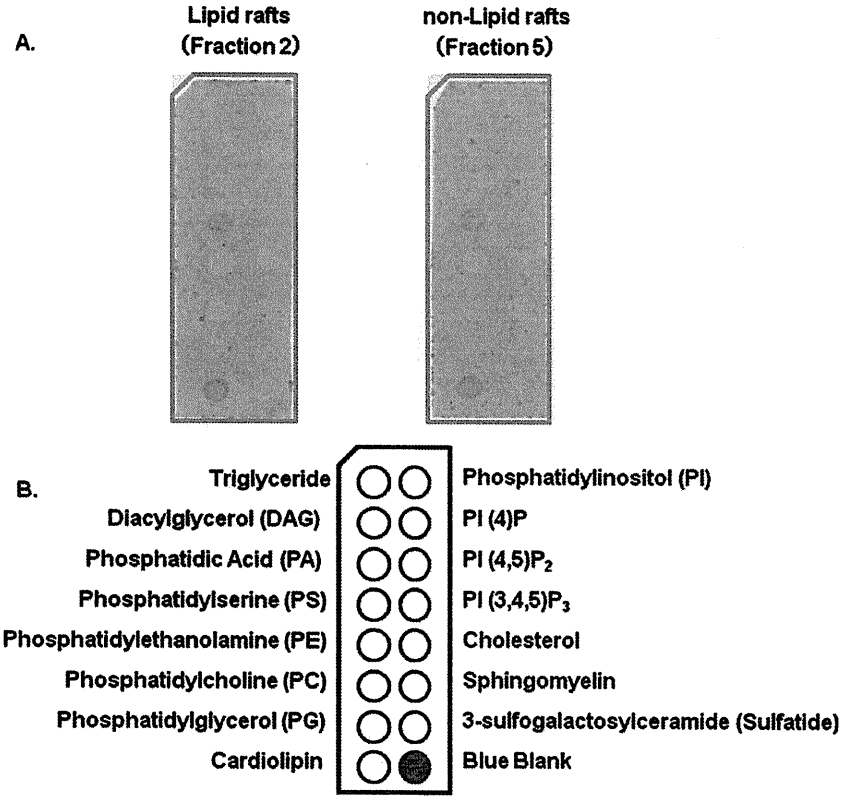

Fig. 5. Interaction of NEP with various lipids. Lipid-attached membrane was treated with sucrose density fractions of SH-SY5Y neuronal cells. After incubation and washing, the membrane was incubated with anti-NEP monoclonal antibody as described in Materials and Methods. The bound NEP was detected by ECL advance. **A:** ECL results. **B:** Lipids attached to the membrane.

Direct Inteaction of NEP With Lipids

The results described above suggest that NEP is localized in lipid rafts, possibly by its direct association with cholesterol. Finally, interaction of NEP with lipids was investigated by using lipid-spotted P-6002 membrane. Fractionated rafts (fraction 2 in Fig. 1A) and nonrafts fractions (fraction 5 in Fig. 1A) were concentrated by ultracentrifugation and incubated with lipids. After washing of the P-6002 membrane, lipid-bound NEP was detected by the specific antibody. Unexpectedly, NEP both in lipid rafts and in nonrafts fractions interacted with phosphatidylserine and cardiolipin but not with cholesterol (Fig. 5).

DISCUSSION

In this study, we found that only the mature form of NEP, glycosylated in the Golgi, and not the immature form, residing in the ER, was localized in lipid rafts (Fig. 1A,B). This indicates that complete glycosylation is required for the association of NEP with lipid rafts. Two possible explanations for this were considered. One is that maturation may be necessary for NEP to bind to a carrier protein such as a glycosylphosphatidylinositol (GPI)-anchored protein. The other is that a small conformational change caused by maturation increases the affinity of NEP for molecules found in lipid rafts, such as sphingolipids and cholesterol. With regard to the former, there have been several reports concerning carrier proteins. One study found that, when the transmembrane and C-terminal domains of BACE1 were replaced with a GPI anchor signal sequence, it was translocated to lipid rafts (Cordy et al., 2003). Another study found that the addition of the N-terminal domain of growth-associated protein 43 (GAP43) to the N-terminus of NEP increased the amount of NEP present in lipid rafts by 1.3-fold (Hama et al., 2004). With regard to the latter possible explanation, we found evidence that the localization of the mature form of NEP in lipid rafts was dependent on the content of cholesterol (Figs. 2, 3). Interestingly, although NEP was completely delocalized by cholesterol depletion, flotillin-1, a lipid raft marker, was not delocalized from lipid rafts by treatment with MβCD (Fig. 2). In this regard, flotillin-1 has been reported to be enriched in detergent-resistant microdomains that are MβCD resistant, although the mechanism

remains to be investigated (Rajendran et al., 2003). Moreover, to examine whether the delocalization of NEP from lipid rafts was caused by its direct association with cholesterol, we extracted lipid raft membranes and treated them with MβCD in vitro (Fig. 3). Consistently with the results presented in Figure 2, NEP was delocalized from lipid rafts membrane by cholesterol depletion, although not completely so (Fig. 3). The difference in the efficiency of NEP delocalization between cell and cell-free systems may be caused by the different conditions used (reaction temperature, membrane state, effects of ultracentrifugation). We conclude that the localization of mature NEP in lipid rafts depends on their cholesterol content.

We investigated the direct association of NEP with pure phospholipids and cholesterol (Fig. 5). Both NEP in rafts and nonrafts directly interacted with phosphatidylserine and cardiolipin. Cardiolipin is a major phospholipid of inner membrane of mammalian mitochondria, so phosphatidylserine might be the major interactor of NEP in lipid rafts. Moreover, immunocytochemical analysis showed that the clustered localization of endogenous NEP in SH-SY5Y cells became dispersed after MβCD treatment (Supp. Info. Fig. 1). Therefore, we conclude that NEP directly associated with phosphatidylserine in cholesterol-rich lipid rafts and MβCD-induced cholesterol depletion triggers the destruction of lipid composition and releases the NEP from rafts. However, the protease activities of mature NEP were unexpectedly comparable in lipid raft and nonlipid raft fractions, as assessed by *p*-NA peptide assay. It is possible that the fractionated lipid rafts did not reflect intracellular conditions (Pike, 2004). However, this result suggests that the association with lipid rafts does not itself modify the protease activity of NEP.

Considering the localization of Aβ in lipid rafts through association with cholesterol (Kakio et al., 2002), we hypothesized that the localization of mature NEP in lipid rafts facilitated its association with Aβ and thereby altered Aβ degradation. Recent studies have shown that lipid raft-dependent endocytosis is the predominant Aβ uptake mechanism (Lai and McLaurin, 2011), that there are correlations between memory deficits and intracellular Aβ levels in several mouse AD models (Billings et al., 2005; Knobloch et al., 2007; Bayer and Wirths, 2008), and that intracellular Aβ level correlates with extracellular amyloid deposition (Yang et al., 2011). Thus, it seems reasonable to conclude that NEP is localized and active in lipid rafts. Indeed, NEP is detected primarily in presynapses and on or around axons in the hippocampal formation (Fukami et al., 2002), and presynaptic NEP efficiently degrades Aβ (Iwata et al., 2004). Considering these findings, together with the fact that the ϵ4 allele of apolipoprotein E (apoE) is a risk factor in nonfamilial AD (Kim et al., 2009), we suggest that cholesterol, overloaded by aging or a high-fat diet, enlarges the area occupied by lipid rafts, thereby decreasing the likelihood of NEP and Aβ coming into contact with each other. As a result, Aβ becomes more abundant, oligomerizes, and causes memory deficits. However, it should be noted that cholesterol itself is a crucial contributor to synaptic structure and function. It has been reported that brain-derived neurotrophic factor (BDNF)-dependent cholesterol biosynthesis plays an important role in synapse development (Suzuki et al., 2007). It would therefore be important to maintain normal cholesterol metabolism during AD therapy.

We further investigated the effects of dimerization on the localization of NEP in lipid rafts. We introduced the E403C mutation into human NEP for the first time. The mutation was originally discovered in rabbit NEP, in which it causes the formation of a covalent homodimer (rabbit NEP normally exists as a monomer). Our results show that human NEP E403C, like rabbit NEP E403C, forms a covalent homodimer. In contrast, human NEP WT, like porcine NEP WT (Kenny et al., 1983), forms a noncovalent homodimer (Fig. 4A,B). Moreover, the noncovalent human NEP WT homodimer, though not resistant to NP-40 or Triton X-100, was resistant to DDM and digitonin. DDM and digitonin dissolve proteins modestly, so the complex remained intact after treatment with these detergents. Interestingly, the localization of mature NEP to lipid rafts was enhanced by its homodimerization (Fig. 4D). With regard to the endopeptidase activity of NEP E403C, Vmax/Km for this mutant was decreased by 50% compared with that for wild-type by using either [D-Ala^2, Leu^5] enkephalin or Suc-Ala-Ala-Leu-NH-Np as a substrate (Hoang et al., 1997). Although the NEP E403C mutant seems to be artificial and to have no physiological significance, these results imply that the protease activity of NEP might be modulated by its dimerization.

In conclusion, we have shown that cholesterol regulates the localization of mature NEP in lipid rafts, where its substrate, Aβ, accumulates. Cholesterol does not, however, modulate the protease activity of NEP.

ACKNOWLEDGMENTS

We thank Dr. Nobuhisa Iwata (Nagasaki University) for providing the protocol for the assay of neprilysin-dependent neutral endopeptidase activity.

REFERENCES

Angelisova P, Drbal K, Horejsi V, Cerny J. 1999. Association of CD10/neutral endopeptidase 24.11 with membrane microdomains rich in glycosylphosphatidylinositol-anchored proteins and Lyn kinase. Blood 93:1437–1439.

Bayer TA, Wirths O. 2008. Review on the APP/PS1KI mouse model: intraneuronal Abeta accumulation triggers axonopathy, neuron loss and working memory impairment. Genes Brain Behav 7(Suppl 1):6–11.

Billings LM, Oddo S, Green KN, McGaugh JL, LaFerla FM. 2005. Intraneuronal Abeta causes the onset of early Alzheimer's disease-related cognitive deficits in transgenic mice. Neuron 45:675–688.

Cordy JM, Hussain I, Dingwall C, Hooper NM, Turner AJ. 2003. Exclusively targeting beta-secretase to lipid rafts by GPI-anchor addition up-regulates beta-site processing of the amyloid precursor protein. Proc Natl Acad Sci U S A 100:11735–11740.

Fukami S, Watanabe K, Iwata N, Haraoka J, Lu B, Gerard NP, Gerard C, Fraser P, Westaway D, St. George-Hyslop P, Saido TC. 2002.

Abeta-degrading endopeptidase, neprilysin, in mouse brain: synaptic and axonal localization inversely correlating with Abeta pathology. Neuroscience research 43:39–56.

Hama E, Shirotani K, Iwata N, Saido TC. 2004. Effects of neprilysin chimeric proteins targeted to subcellular compartments on amyloid beta peptide clearance in primary neurons. J Biol Chem 279:30259–30264.

Hardy JA, Higgins GA. 1992. Alzheimer's disease: the amyloid cascade hypothesis. Science 256:184–185.

Hellstrom-Lindahl E, Ravid R, Nordberg A. 2008. Age-dependent decline of neprilysin in Alzheimer's disease and normal brain: inverse correlation with A beta levels. Neurobiol Aging 29:210–221.

Hoang MV, Sansom CE, Turner AJ. 1997. Mutagenesis of Glu403 to Cys in rabbit neutral endopeptidase-24.11 (neprilysin) creates a disulphide-linked homodimer: analogy with endothelin-converting enzyme. Biochem J 327:925–929.

Iwata N, Tsubuki S, Takaki Y, Shirotani K, Lu B, Gerard NP, Gerard C, Hama E, Lee HJ, Saido TC. 2001. Metabolic regulation of brain Abeta by neprilysin. Science 292:1550–1552.

Iwata N, Takaki Y, Fukami S, Tsubuki S, Saido TC. 2002. Region-specific reduction of A beta-degrading endopeptidase, neprilysin, in mouse hippocampus upon aging. J Neurosci Res 70:493–500.

Iwata N, Mizukami H, Shirotani K, Takaki Y, Muramatsu S, Lu B, Gerard NP, Gerard C, Ozawa K, Saido TC. 2004. Presynaptic localization of neprilysin contributes to efficient clearance of amyloid-beta peptide in mouse brain. J Neurosci 24:991–998.

Kakio A, Nishimoto S, Yanagisawa K, Kozutsumi Y, Matsuzaki K. 2002. Interactions of amyloid beta-protein with various gangliosides in raft-like membranes: importance of GM1 ganglioside-bound form as an endogenous seed for Alzheimer amyloid. Biochemistry 41:7385–7390.

Kanemitsu H, Tomiyama T, Mori H. 2003. Human neprilysin is capable of degrading amyloid beta peptide not only in the monomeric form but also the pathological oligomeric form. Neurosci Lett 350:113–116.

Kawarabayashi T, Shoji M, Younkin LH, Wen-Lang L, Dickson DW, Murakami T, Matsubara E, Abe K, Ashe KH, Younkin SG. 2004. Dimeric amyloid beta protein rapidly accumulates in lipid rafts followed by apolipoprotein E and phosphorylated tau accumulation in the Tg2576 mouse model of Alzheimer's disease. J Neurosci 24:3801–3809.

Kenny AJ, Fulcher IS, McGill KA, Kershaw D. 1983. Proteins of the kidney microvillar membrane. Reconstitution of endopeptidase in liposomes shows that it is a short-stalked protein. Biochem J 211:755–762.

Kim J, Basak JM, Holtzman DM. 2009. The role of apolipoprotein E in Alzheimer's disease. Neuron 63:287–303.

Knobloch M, Konietzko U, Krebs DC, Nitsch RM. 2007. Intracellular Abeta and cognitive deficits precede beta-amyloid deposition in transgenic arcAbeta mice. Neurobiol Aging 28:1297–1306.

Kojro E, Gimpl G, Lammich S, Marz W, Fahrenholz F. 2001. Low cholesterol stimulates the nonamyloidogenic pathway by its effect on the alpha-secretase ADAM 10. Proc Natl Acad Sci U S A 98:5815–5820.

Lafrance MH, Vezina C, Wang Q, Boileau G, Crine P, Lemay G. 1994. Role of glycosylation in transport and enzymic activity of neutral endopeptidase-24.11. Biochem J 302:451–454.

Lai AY, McLaurin J. 2011. Mechanisms of amyloid-beta peptide uptake by neurons: the role of lipid rafts and lipid raft-associated proteins. Int J Alzheimers Dis 2011:548380.

Matsuzaki K, Noguch T, Wakabayashi M, Ikeda K, Okada T, Ohashi Y, Hoshino M, Naiki H. 2007. Inhibitors of amyloid beta-protein aggregation mediated by GM1-containing raft-like membranes. Biochim Biophys Acta 1768:122–130.

Pike LJ. 2004. Lipid rafts: heterogeneity on the high seas. Biochem J 378:281–292.

Pike LJ. 2006. Rafts defined: a report on the Keystone Symposium on Lipid Rafts and Cell Function. J Lipid Res 47:1597–1598.

Rajendran L, Masilamani M, Solomon S, Tikkanen R, Stuermer CA, Plattner H, Illges H. 2003. Asymmetric localization of flotillins/reggies in preassembled platforms confers inherent polarity to hematopoietic cells. Proc Natl Acad Sci U S A 100:8241–8246.

Riemann D, Hansen GH, Niels-Christiansen L, Thorsen E, Immerdal L, Santos AN, Kehlen A, Langner J, Danielsen EM. 2001. Caveolae/lipid rafts in fibroblast-like synoviocytes: ectopeptidase-rich membrane microdomains. Biochem J 354:47–55.

Selkoe DJ. 2002. Alzheimer's disease is a synaptic failure. Science 298:789–791.

Suzuki S, Kiyosue K, Hazama S, Ogura A, Kashihara M, Hara T, Koshimizu H, Kojima M. 2007. Brain-derived neurotrophic factor regulates cholesterol metabolism for synapse development. J Neurosci 27:6417–6427.

von Tresckow B, Kallen KJ, von Strandmann EP, Borchmann P, Lange H, Engert A, Hansen HP. 2004. Depletion of cellular cholesterol and lipid rafts increases shedding of CD30. J Immunol 172:4324–4331.

Wada S, Morishima-Kawashima M, Qi Y, Misono H, Shimada Y, Ohno-Iwashita Y, Ihara Y. 2003. Gamma-secretase activity is present in rafts but is not cholesterol-dependent. Biochemistry 42:13977–13986.

Yang DS, Stavrides P, Mohan PS, Kaushik S, Kumar A, Ohno M, Schmidt SD, Wesson D, Bandyopadhyay U, Jiang Y, Pawlik M, Peterhoff CM, Yang AJ, Wilson DA, St. George-Hyslop P, Westaway D, Mathews PM, Levy E, Cuervo AM, Nixon RA. 2011. Reversal of autophagy dysfunction in the TgCRND8 mouse model of Alzheimer's disease ameliorates amyloid pathologies and memory deficits. Brain 134:258–277.

Neuroscience Letters 503 (2011) 234–239

Contents lists available at SciVerse ScienceDirect

Neuroscience Letters

journal homepage: www.elsevier.com/locate/neulet

Protective role of the ubiquitin binding protein Tollip against the toxicity of polyglutamine-expansion proteins

Asami Oguro[a,1], Hiroshi Kubota[b], Miho Shimizu[c], Shoichi Ishiura[a], Yoriko Atomi[d,*]

[a] Department of Life Sciences, The Graduate School of Arts and Sciences, The University of Tokyo, Meguro-ku, Tokyo 153-8902, Japan
[b] Department of Life Science, Faculty and Graduate School of Engineering and Resource Science, Akita University, 1-1 Tegatagakuen-cho, Akita 010-8502, Japan
[c] Graduate School of Information Science and Technology, The University of Tokyo, 7-3-1, Hongo, Bunkyo-ku, Tokyo 113-8656, Japan
[d] The University of Tokyo, Radioisotope Center Cell to Body Dynamics Laboratory 1 2-11-16, Yayoi, Bunkyo-ku, Tokyo 113-0032, Japan

ARTICLE INFO

Article history:
Received 7 January 2011
Received in revised form 3 August 2011
Accepted 22 August 2011

Keywords:
Aggregation
Huntingtin
Polyglutamine
Tollip

ABSTRACT

Huntington disease (HD) is caused by the expansion of polyglutamine (polyQ) repeats in the amino-terminal of hungtintin (htt). PolyQ-expanded htt forms intracellular ubiquitinated aggregates in neurons and causes neuronal cell death. Here, utilizing a HD cellular model, we report that Tollip, an ubiquitin binding protein that participates in intracellular transport *via* endosomes, co-localizes with and stimulates aggregation of polyQ-expanded amino-terminal htt. Furthermore, we demonstrate that Tollip protects cells against the toxicity of polyQ-expanded htt. We propose that association of Tollip with polyubiquitin accelerates aggregation of toxic htt species into inclusions and thus provides a cell protective role by sequestration.

Huntington disease (HD, OMIM-143100) is a progressive autosomal dominant neurodegenerative disorder caused by expansion of polyglutamine (polyQ) in the hungtintin (htt) protein. The gene encoding htt contains a CAG repeat in exon 1, and this repeat is expanded in HD patients. Although full-length htt is ubiquitously expressed as a 348-kDa cytoplasmic protein, the amino-terminal fragments of polyQ expanded htt (htt^{pQ}) tend to form ubiquitinated intracellular aggregates and exert toxicity in neuronal cells [1]. Htt^{pQ} has been shown to cause protein misfolding, aberrant transcription, chaperone activity inhibition and proteasome dysfunction, although the exact molecular mechanism by which polyQ exerts cellular toxicity is unknown [8].

Tollip (Toll-interacting protein) is a ubiquitin binding protein that is involved in sorting of ubiquitinated proteins from endosomes to lysosomes for degradation including that of interleukin-1 receptor (IL-1R) [3,4]. Tollip binds to ubiquitin through the CUE (coupling of ubiquitin to ER degradation) domain and interacts with clathrin and Tom1 (target of Myb protein 1), leading to formation of a multi protein complex for protein degradation [9]. Tollip is localized in endosomes, and disruption of the *Tollip* gene results in accumulation of IL-1R in endosomes and deficiency in lysosomal degradation of IL-1R [3]. Tollip is reported as a protein concentrated in polyglutamine aggregates [5], and the ubiquitin binding protein p62 (also known as sequestosome 1) is known to mediate autophagy-dependent clearance of polyQ aggregates with accelerating htt^{pQ} aggregation [13]. These observations suggested that, like p62, Tollip may be involved in htt^{pQ} aggregation and degradation through ubiquitin binding and membrane sorting activities. Thus, we decided to analyze the role of Tollip in htt^{pQ} aggregation, trafficking and cytotoxicity in neuronal cells.

Experimental procedures: The *htt* expression constructs, pIND-tNhtt-EGFP-60Q and pIND-tNhtt-EGFP-150Q, and the generation of the stable Neuro2a cell lines expressing htt proteins were provided by Dr. Nukina [7]. The stable cell lines (HD60Q and HD150Q) were maintained in DMEM supplemented with 10% fetal bovine serum, 0.4 mg/ml Zeocin and 0.4 mg/ml G418 (Sigma). All transfections were performed using the Lipofectamine 2000 reagent (Invitrogen) according to the manufacturer's instructions. To knockdown *Tollip*, cells were transiently transfected with *Tollip* stealth siRNA duplex oligoribonucleotides, 5′-UCUCAAGGUAGAACGAGUCCACACC-3′ and 5′-GGUGUGGACUCGUUCUACCUUGAGA-3′ or Stealth RNAi Negative Control Duplexes, while *Tollip* overexpression was achieved by transiently transfected with the RFP-Tollip expression vector [mouse *Tollip* cloned into the RFPc1 vector (Invitrogen)]. To assess if levels of *Tollip* affected aggregate formation, cells were transiently cotransfected with either GFP-Tollip (or empty GFP cassette) and *htt* (20Q, 80Q or 87Q) exon1 fused with a V5 tag. Twelve hours after transfection, 1 μM of ponasterone A (Invitrogen) for induction of

* Corresponding author. Tel.: +81 3 5841 3055; fax: +81 3 5841 3055.
E-mail addresses: oguroasami@ucla.edu (A. Oguro), hkubota@ipc.akita-u.ac.jp (H. Kubota), mshimizu@ynl.t.u-tokyo.ac.jp (M. Shimizu), cishiura@mail.ecc.u-tokyo.ac.jp (S. Ishiura), atomi@bio.c.u-tokyo.ac.jp (Y. Atomi).
[1] Present address: Department of Neurology, David Geffen School of Medicine, University of California, Los Angeles, CA 90095, USA.

0304-3940/$ – see front matter © 2011 Elsevier Ireland Ltd. All rights reserved.
doi:10.1016/j.neulet.2011.08.043

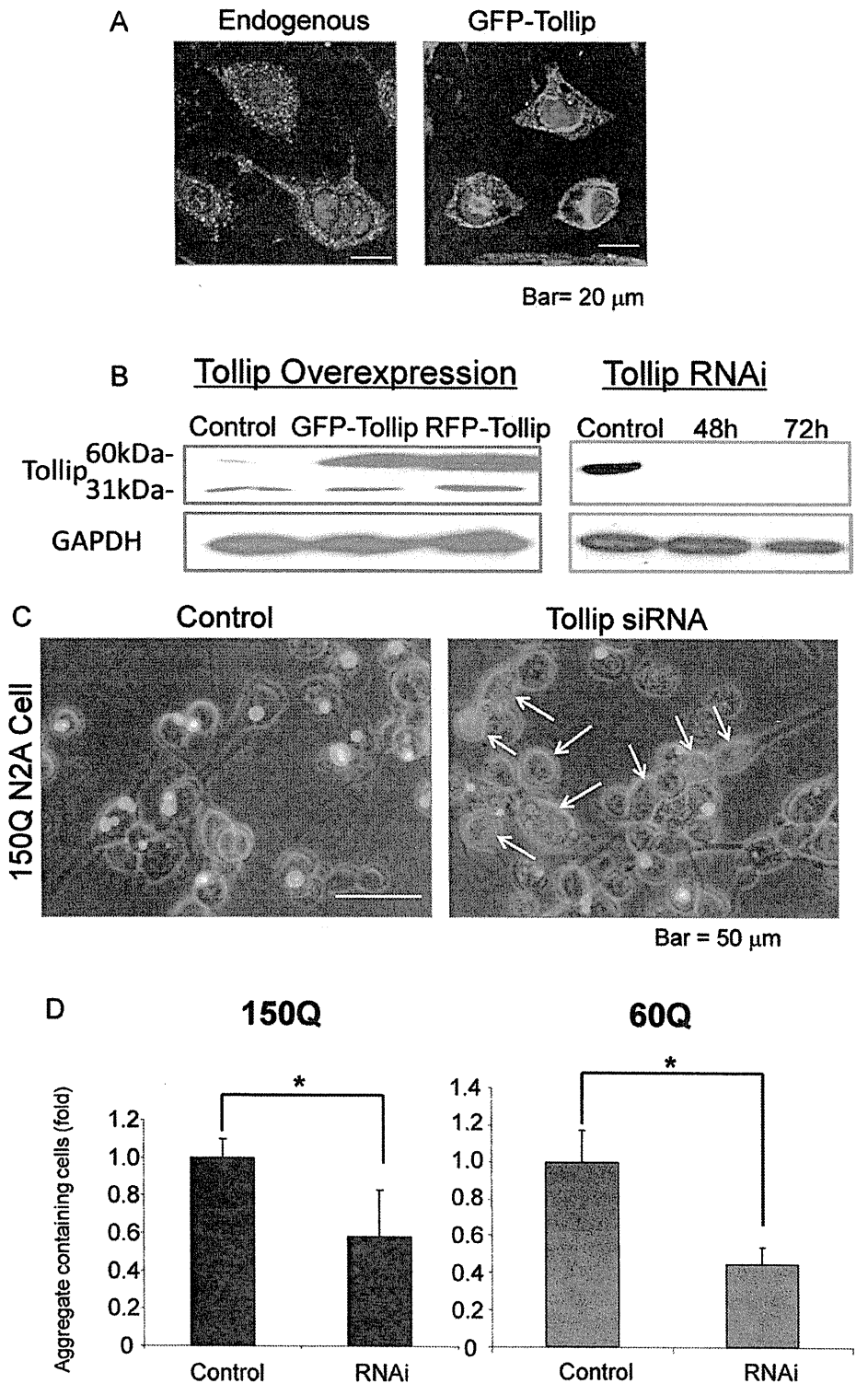

Fig. 1. Tollip associates with aggregates of polyQ-expanded htt and affects polyQ aggregation. (A) GFP-Tollip overexpression shows the same localization pattern as endogenous Tollip in the htt150Q Neuro2a cell line without induction. At 48 h of transfection, cells were analyzed by immunostaining. Tollip distributed in small granular particles in the cytoplasm. Bar = 20 μm. (B) Cells were transiently transfected with GFP-*Tollip* or RFP-*Tollip* for 48 h (left), or *Tollip* siRNA for 48–72 h (right). Tollip expression level was analyzed by Western blotting. (C) Htt150Q-expressing cells were transfected with *Tollip* siRNA or control siRNA for 48 h. *Tollip* siRNA treated cells exhibits decreased htt^{pQ} aggregation. Arrows indicate GFP-positive cells that do not form htt^{pQ} aggregates. Bar = 50 μm. (D) *Tollip* knockdown inhibits htt^{pQ} aggregation. HD150Q and HD60Q cells were transfected with *Tollip* siRNA or control siRNA, and aggregate-containing cells were counted ($n = 3$). *, $p < 0.01$.

aggregation was added to the culture and then incubated for an additional 24 h. To count aggregate containing cells, 1×10^3 cells were seeded into chambered slides, and aggregate containing cells were manually counted using a fluorescence microscope. To test cell death, 5×10^5 cells were inoculated into each well of 6-well plates, 48 h following transfection, cells were differentiated with 5 mM dibutyryl cyclic AMP in the presence of 1 μM of ponasterone A and allowed to incubate for three days. Aggregate counting experiments were performed after cells were transiently transfected with *Tollip* stealth siRNA duplex or plasmid expression vector (transfection efficiency was almost 90% in Neuro2a cells), and more than 200 cells were counted. Dead cells were counted by propidium iodide staining as described previously [10], and cell viability was measured using Titer Blue assay kit (Promega). Statistical analysis was performed by Student's *t*-test. To inhibit the proteasome, cells were treated with carbobenzoxy-L-leucyl-L-leucyl-L-leucinal (MG-132; Wako, Osaka, Japan) and microtubule destabilization was performed using nocodazole (Sigma).

For immunofluorescence experiments, cells were fixed with 4% paraformaldehyde in PBS for 20 min and blocked with 0.2% BSA in TBST (Tris-Buffered Saline Tween-20) for 1 h. Fixed cells were incubated with antibodies against Tollip (rabbit polyclonal, Ref. [21]), vimentin (mouse monoclonal, Abcam), EEA1 (mouse monoclonal, BD Transduction) or syntaxin-7 (rabbit polyclonal, Abcam) at 1:50 dilution (4 °C, overnight). After several washes with TBST, cells were incubated with Alexa488- or Alexa546-conjigated secondary antibodies (1:2000) for 1 h. After washes, cells were mounted in antifade solution. Immunofluoresent staining of Tollip in HD150Q cells was carried out as described [7]. Solubility of proteins was examined as follows: cells were scraped, homogenized and lysed in PBS supplemented with protease inhibitor cocktail (Sigma) on ice. Cell lysates were briefly sonicated, centrifuged for 10 min at 15,000 × *g* at 4 °C, and supernatants (soluble fraction) and pellet (insoluble fraction) were analyzed by Western blotting [21].

To examine whether Tollip affects htt^{PQ} aggregation, we established Tollip overexpression and knockdown system *in vitro* (Fig. 1A and B). After overexpression of Tollip using GFP-Tollip construct, transfected Neuro2a cells showed essentially the same localization pattern as endogenous Tollip in cytosol (Fig. 1A), while expression levels of GFP/RFP-Tollip were significantly higher than endogenous Tollip (Fig. 1B, left). Treatment of Neuro2a cells with *Tollip* siRNA diminished endogenous Tollip protein after 48 h through 72 h (Fig. 1B, right). Under the Tollip knockdown conditions, the number of cells that contain htt (150Q and 60Q) aggregates was significantly reduced to approximately 50% (Fig. 1C and D). These results indicate that Tollip stimulates polyQ aggregation in living cells.

Since many polyQ binding proteins affects polyQ-dependent cell death [18], we hypothesized that association of Tollip with htt^{PQ} aggregates may affect polyQ toxicity. Overexpression of Tollip significantly stimulated aggregation of GFP-htt60Q (Fig. 2A), and suppressed cell death in the htt80Q and htt87Q lines (Fig. 2B). In contrast, Tollip overexpression provided no significant difference on the cell death of htt20Q expressing cells (Fig. 2B). Thus, Tollip protects cells against the toxicity of expanded polyQ concomitant with stimulating htt^{PQ} aggregation into aggresomes.

Previous reports indicated that Tollip contains the ubiquitin binding CUE domain [15,20]. Ubiquitin binding motifs are also found in p62 and ubiquilin1, and these proteins function in the ubiquitin–proteasome pathway [6,18]. To investigate whether Tollip distribution is affected by proteasomal inhibition, Neuro2a cells treated with the proteasome inhibitor MG-132 and localization of Tollip was analyzed by immunofluorescence microscopy (Fig. 3A). MG-132 treatment frequently induced formation of juxtanuclear Tollip-containing inclusions surrounded by vimentin, of which specific structure is a marker of the aggresome. We next treated cells

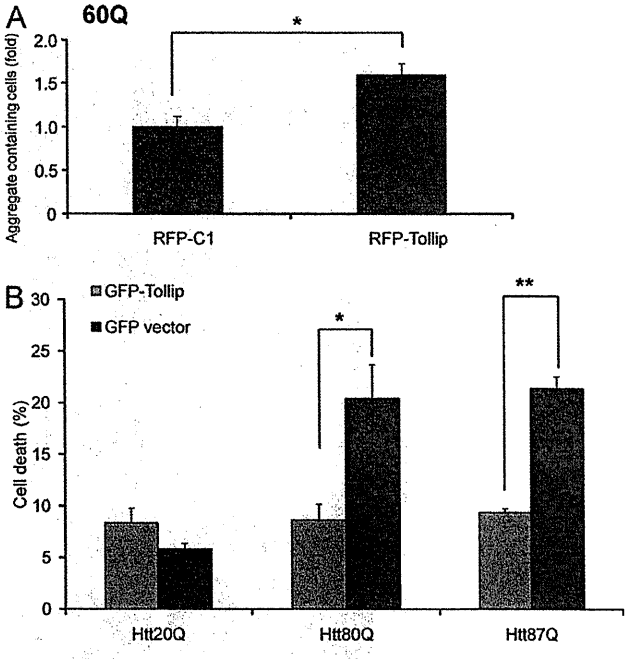

Fig. 2. Overexpression of Tollip induces htt^{PQ} aggregation and reduces cell death. (A) Htt-expressing cells were transfected with RFP-Tollip or RFP-C as a control, and aggregate-containing cells were counted ($n = 4$). (B) Tollip protects cells against the toxicity of htt^{PQ}. Neuro2a cells were transiently co-transfected with htt (20Q, 80Q or 87Q) and GFP-Tollip (or GFP as a control). Cells were differentiated in the presence of 5 mM dbcAMP. Cell death was analyzed by propidium iodide staining ($n = 4$). More than 300 cells were counted for each experiment. *, $p < 0.01$; **, $p < 0.001$.

with the microtubule-destabilizing drug nocodazole, because formation and maintenance of aggresomes are known to be dependent on microtubule-dependent transport system. Treatment of cells with nocodazole resulted in a more dispersed distribution of Tollip in the cytoplasm in the presence of MG-132. These results indicate that Tollip is concentrated in the aggresome and/or in the region surrounding the aggresome. Centrifugal fractionation indicated that Tollip was present in the insoluble fractions after MG132 treatment (Fig. 3B). Given the insoluble nature of the aggresome, this suggests that Tollip is associated with this structure.

Tollip is known to play a role in endosomal protein trafficking; therefore we performed immunostaining of Tollip with EEA1 (an early endosome marker) or syntaxin-7 (a late endosome marker) in cultured Neuro2a and HEK293 cells after treatment with MG-132 (Fig. 4A). Tollip was rarely found in early endosomes but partly distributed in late endosomes under normal conditions. After MG132 treatment, however, Tollip was highly colocalized with the late endosome marker syntaxin-7. Previous studies indicated that Tollip is known to be accumulated in htt^{PQ} inclusions in the brain of HD model mouse (R6/1) [21]. We thus tested whether Tollip associates with htt^{PQ} aggregates in the HD cellular model [7]. Expression of GFP-htt150Q was induced for 24 h in the presence of ponasterone A, and localization of Tollip was analyzed by immunofluorescence staining. Strong Tollip staining surrounding htt^{PQ} aggregates was observed (Fig. 4B, upper). We also analyzed localization of syntaxin-7 in htt150Q expressing cells and found that syntaxin-7 colocalizes with htt^{PQ} aggregates (Fig. 4B, lower). Thus, Tollip function may be associated with recruitment of misfolded proteins to aggresomes *via* late endosomes, including the case of htt^{PQ}. Under MG132-induced stress conditions, overexpression of Tollip significantly protected cells from the toxicity of the proteasome inhibitor (Fig. 4C, left). Furthermore, knockdown of Tollip significantly decreased cell viability of MG132-treated cells (Fig. 4C, right). These results indicate that

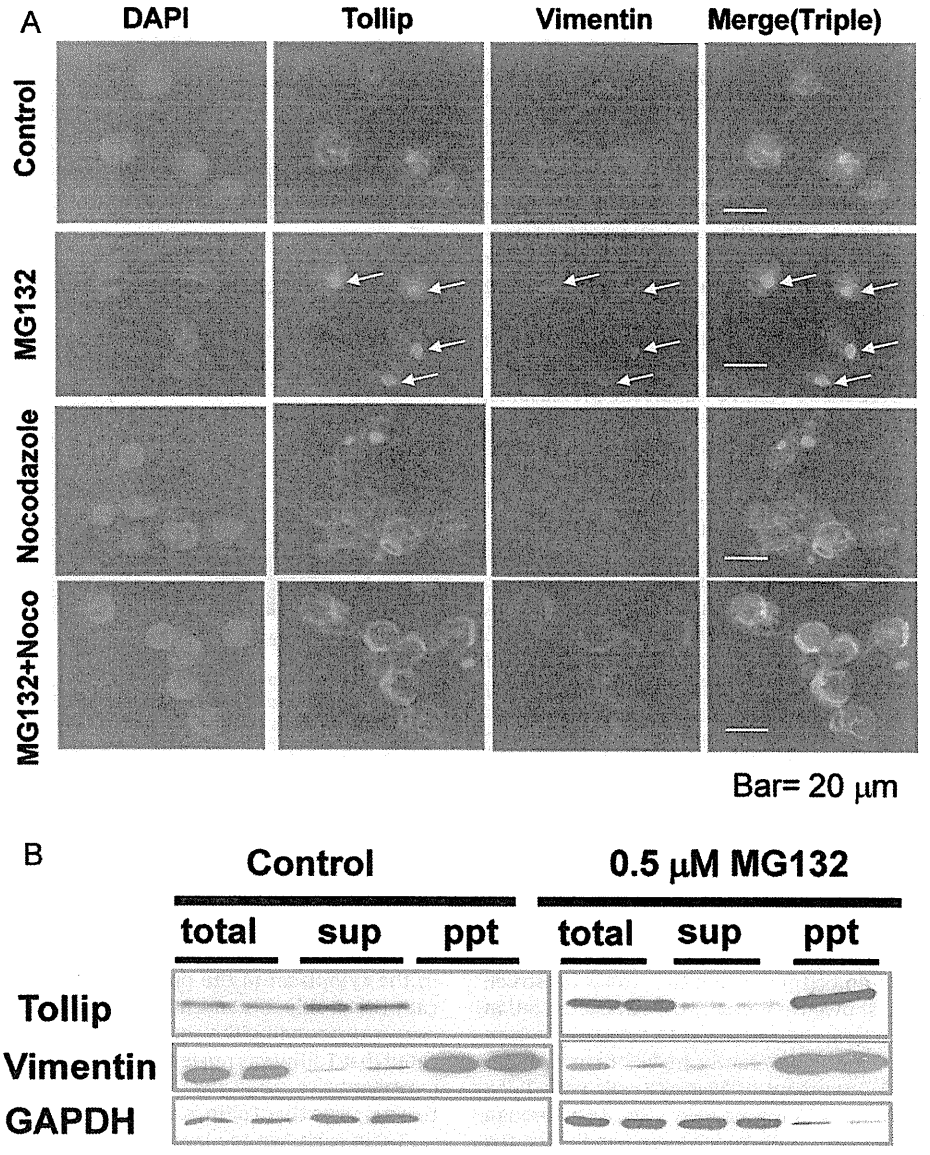

Fig. 3. Proteasome inhibition causes accumulation of Tollip in the aggresome. (A) After treatment with 0.5 μM MG-132 for 24 h, cells were stained with antibodies against Tollip and vimentin. Arrows indicate aggresomes surrounded by vimentin cage in Neuro2a cells. Alternatively, after treatment of Neuro2a cells with 10 μM nocodazole and 0.5 μM MG-132 for 12 h, cells were analyzed by immunostaining. Tollip exhibited multiple, small and granular distribution in the cytoplasm after nocodazole treatment. Bar = 20 μm. (B) Western blot analysis of soluble (sup) and insoluble (ppt) fractions prepared from Neuro2a cells after treatment with MG-132 for 24 h or untreated as a control. Blotted proteins were analyzed with indicated antibodies.

Tollip is required for maintaining cell viability against the toxicity of misfolded proteins, probably by recruiting them to aggresomes.

The formation of intracellular ubiquitinated aggregates is a hallmark of polyQ diseases including HD. Transcription factors, molecular chaperones and ubiquitin–proteasome system proteins are known to associate with the polyQ aggregates and implicated in the pathogenesis of polyQ disease [18]. However, role of aggregation in the toxicity is controversial, because accumulating evidence suggests that controlled aggregation into inclusion bodies has cell protective roles against misfolded proteins including polyQ-expanded proteins [16,17]. Tollip is involved in two major cascades of cellular functions. Firstly, Tollip interacts with the TIR domain of the IL-1R [4]. Since the TIR domain mediates the binding of the serine/threonine kinase IRAK-1 to the activated receptor complex, Tollip acts as a regulator of the signaling cascade. Secondly, Tollip is known to interact with polyubiquitinated proteins through the CUE domain and is involved in the ubiquitin–proteasome system. In the case of IL-1R, the CUE domain and TIR interacting domain of Tollip are required for endosome-mediated lysosomal degradation of IL-1R [3]. In the present study, we analyzed the role of Tollip in htt^{PQ} aggregation and cytotoxicity and found that Tollip associates with the htt^{PQ} aggregates and protect cells against htt^{PQ} toxicity by stimulating aggregation (Figs. 1 and 2).

Tollip is a multifunctional protein that interacts with a number of ubiquitin-related proteins and sumolylated proteins, and forms a complex with TOM1, polyubiquitin chains and clathrin heavy chain [9]. As Tollip localizes in endosomes [3], Tollip can function as a molecular link between endosomal processing and ubiquitin–proteasome system. In the present study, we demonstrate that Tollip colocalizes with a late endosome marker in htt^{PQ} aggregates and the aggresome formed under proteasome inhibition

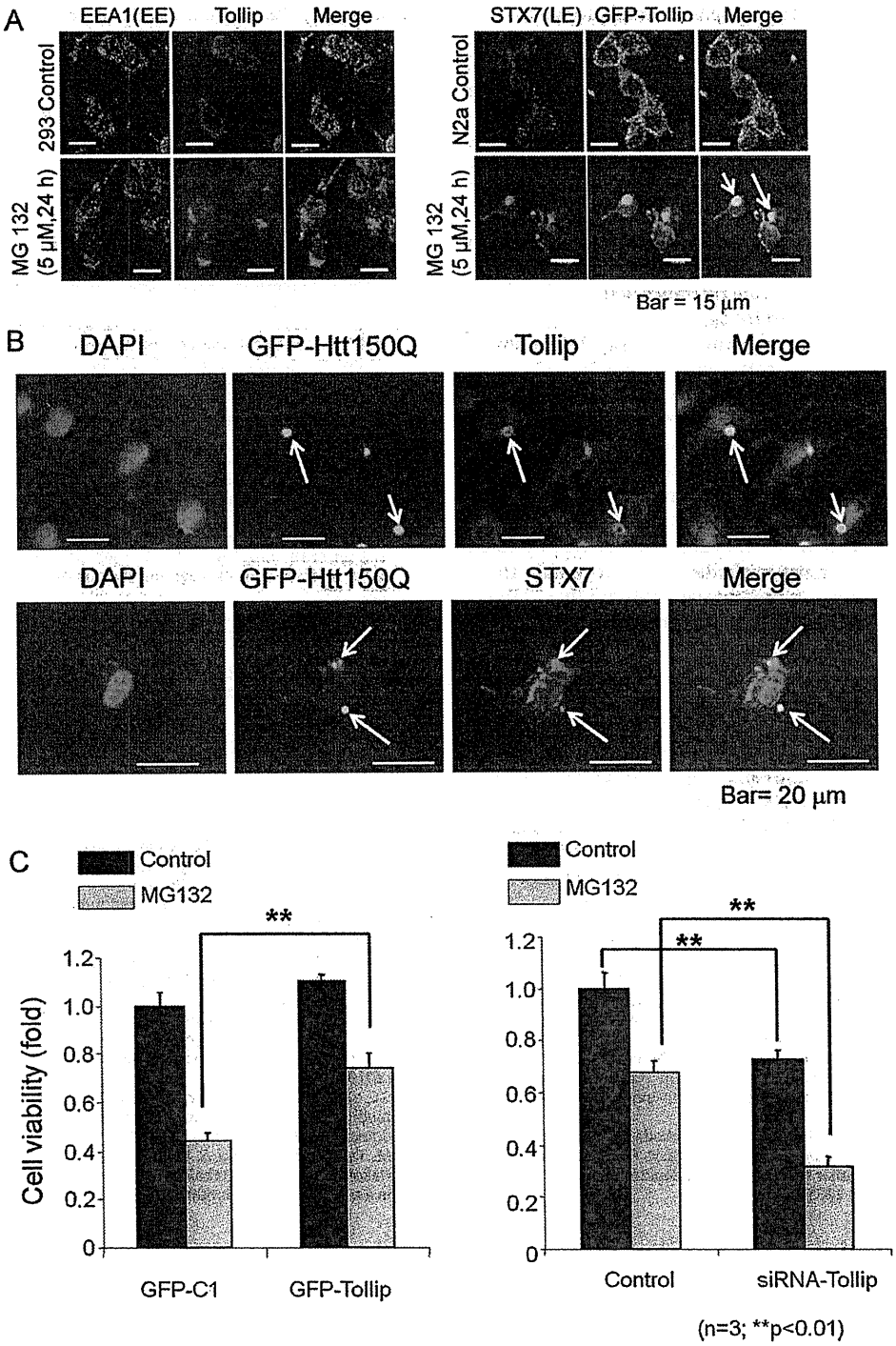

Fig. 4. Colocalization of Tollip with a late endosomal maker in MG132-induced aggresomes and htt^{pQ} inclusions and Tollip-dependent cell protection against the toxicity of proteasome inhibition. (A) HEK293 cells were co-stained with antibodies against EEA1 (early endosome marker) and Tollip (left), or GFP-Tollip transfected Neuro2a cells were stained with antibody against syntaxin-7 (late endosome marker) (right). Arrows indicate the co-localization of Tollip with syntaxin-7. Bar = 15 μm. (B) A Neuro2a cell line stably expressing GFP-htt150Q was stained with anti-Tollip (upper) or anti-syntaxin-7 (lower) antibodies. Arrows indicate the co-localization of Tollip and syntaxin-7 in htt aggregates. Bar = 20 μm. (C) After the treatment with 5 μM MG-132 for 24 h, Neuro2a cells were transiently transfected with GFP-Tollip or GFP vector as a control (left). Alternatively, cells were treated with *Tollip* siRNA or control siRNA as a control (right). Cells were then differentiated in the presence of 5 mM dbcAMP. Cell viability was measured by Titer Blue assay (Promega) ($n = 3$). **, $p < 0.001$. The difference of control cell viability between left and right panels is considered to be due to the difference in toxic effect between plasmid DNA transfection and small RNA transfection [11].

conditions (Figs. 3 and 4). These observations strongly suggest that Tollip mediates trafficking of ubiquitinated aberrant proteins to aggresomes *via* late endosomes or structures containing endosomal proteins.

Accumulating evidence indicates that ubiquitin binding proteins play crucial roles in degradation of polyQ proteins through ubiquitin and autophagy systems. For example, the ubiquitin binding protein p62 co-localizes with many types of polyubiquitinated

protein aggregates and recruit the autophagosomal protein LC3 [2]. The p62 protein recognizes polyubiquitin by the carboxyl-terminal UBA domain and is polymerized through the amino-terminal PB1 domain. Expression of p62 is strongly induced by exposure to proteasomal inhibitors or overexpression of polyglutamine-expanded proteins [18], and this protein is required for autophagic clearance of misfolded proteins [2,11,12]. Ubiquilin, another ubiquitin binding protein, protects cells against the toxicity of htt exon-1 (74Q) through authophagy [19]. Formation of inclusions/aggresomes is considered to reduce toxic misfolded species like oligomers, and ubiquitin interacting proteins may stimulate formation of aggresomes to accelerate clearance of the toxic species by microtubule-dependent controlled aggregation and degradation through the autophagy–lysosome pathway [11,14]. These observations suggest that Tollip protects cells perhaps by enhancing controlled aggregation to the aggresome using the ubiquitin binding CUE domain and the ability to interact with multiple proteins (e.g., clathrin and Tom1). Since Tollip is involved in protein transport *via* endosomes [9] and Tollip colocalized with an endosome maker in aggresomes/inclusions in our experiments, Tollip may accerelate aggregation of ubiquitinated proteins *via* endosomes, although precise roles of Tollip in the aggregation of ubiquitinated proteins and protection against misfolded proteins remain to be investigated. In conclusion, our present data indicate that Tollip is a cell protective ubiquitin binding protein that stimulates aggresome/inclusion formation in neuronal cells.

Acknowledgements

We thank Dr. Nobuyuki Nukina (RIKEN Brain Institute) for kindly providing htt expressing cell lines and helpful discussion. We also thank Drs. Takashi Tsuboi (University of Tokyo) for providing helpful ideas, Kouta Kanno (University of Tokyo) for helping htt plasmid preparation and Brent Bill (UCLA) for giving helpful advice. AO was supported by a fellowship from Japan Society for Promotion of Science.

References

[1] The Huntington's Disease Collaborative Research Group, A novel gene containing a trinucleotide repeat that is expanded and unstable on Huntington's disease chromosomes, Cell 72 (1993) 971–983.
[2] G. Bjorkoy, T. Lamark, A. Brech, H. Outzen, M. Perander, A. Overvatn, H. Stenmark, T. Johansen, p62/SQSTM1 forms protein aggregates degraded by autophagy and has a protective effect on huntingtin-induced cell death, J. Cell Biol. 171 (2005) 603–614.
[3] B. Brissoni, L. Agostini, M. Kropf, F. Martinon, V. Swoboda, S. Lippens, H. Everett, N. Aebi, S. Janssens, E. Meylan, M. Felberbaum-Corti, H. Hirling, J. Gruenberg, J. Tschopp, K. Burns, Intracellular trafficking of interleukin-1 receptor I requires Tollip, Curr. Biol. 16 (2006) 2265–2270.
[4] K. Burns, J. Clatworthy, L. Martin, F. Martinon, C. Plumpton, B. Maschera, A. Lewis, K. Ray, J. Tschopp, F. Volpe, Tollip a new component of the IL-1RI pathway, links IRAK to the IL-1 receptor, Nat. Cell Biol. 2 (2000) 346–351.
[5] H. Doi, K. Mitsui, M. Kurosawa, Y. Machida, Y. Kuroiwa, N. Nukina, Identification of ubiquitin-interacting proteins in purified polyglutamine aggregates, FEBS Lett. 571 (2004) 171–176.
[6] R. Heir, C. Ablasou, E. Dumontier, M. Elliott, C. Fagotto-Kaufmann, F.K. Bedford, The UBL domain of PLIC-1 regulates aggresome formation, EMBO Rep. 7 (2006) 1252–1258.
[7] N.R. Jana, N. Nukina, BAG-1 associates with the polyglutamine-expanded huntingtin aggregates, Neurosci. Lett. 378 (2005) 171–175.
[8] N.R. Jana, E.A. Zemskov, G. Wang, N. Nukina, Altered proteasomal function due to the expression of polyglutamine-expanded truncated N-terminal huntingtin induces apoptosis by caspase activation through mitochondrial cytochrome c release, Hum. Mol. Genet. 10 (2001) 1049–1059.
[9] Y. Katoh, Y. Shiba, H. Mitsuhashi, Y. Yanagida, H. Takatsu, K. Nakayama, Tollip and Tom1 form a complex and recruit ubiquitin-conjugated proteins onto early endosomes, J. Biol. Chem. 279 (2004) 24435–24443.
[10] A. Kitamura, H. Kubota, C.G. Pack, G. Matsumoto, S. Hirayama, Y. Takahashi, H. Kimura, M. Kinjo, R.I. Morimoto, K. Nagata, Cytosolic chaperonin prevents polyglutamine toxicity with altering the aggregation state, Nat. Cell Biol. 8 (2006) 1163–1170.
[11] M. Komatsu, Y. Ichimura, Physiological significance of selective degradation of p62 by autophagy, FEBS Lett. 584 (2010) 1374–1378.
[12] M. Komatsu, H. Kurokawa, S. Waguri, K. Taguchi, A. Kobayashi, Y. Ichimura, Y.S. Sou, I. Ueno, A. Sakamoto, K.I. Tong, M. Kim, Y. Nishito, S. Iemura, T. Natsume, T. Ueno, E. Kominami, H. Motohashi, K. Tanaka, M. Yamamoto, The selective autophagy substrate p62 activates the stress responsive transcription factor Nrf2 through inactivation of Keap1, Nat. Cell Biol. 12 (2010) 213–223.
[13] M. Komatsu, S. Waguri, M. Koike, Y.S. Sou, T. Ueno, T. Hara, N. Mizushima, J. Iwata, J. Ezaki, S. Murata, J. Hamazaki, Y. Nishito, S. Iemura, T. Natsume, T. Yanagawa, J. Uwayama, E. Warabi, H. Yoshida, T. Ishii, A. Kobayashi, M. Yamamoto, Z. Yue, Y. Uchiyama, E. Kominami, K. Tanaka, Homeostatic levels of p62 control cytoplasmic inclusion body formation in autophagy-deficient mice, Cell 131 (2007) 1149–1163.
[14] R.R. Kopito, Aggresomes, inclusion bodies and protein aggregation, Trends Cell Biol. 10 (2000) 524–530.
[15] Y.L. Lo, A.G. Beckhouse, S.L. Boulus, C.A. Wells, Diversification of TOLLIP isoforms in mouse and man, Mamm. Genome 20 (2009) 305–314.
[16] R. Luthi-Carter, D.M. Taylor, J. Pallos, E. Lambert, A. Amore, A. Parker, H. Moffitt, D.L. Smith, H. Runne, O. Gokce, A. Kuhn, Z. Xiang, M.M. Maxwell, S.A. Reeves, G.P. Bates, C. Neri, L.M. Thompson, J.L. Marsh, A.G. Kazantsev, SIRT2 inhibition achieves neuroprotection by decreasing sterol biosynthesis, Proc. Natl. Acad. Sci. U.S.A. 107 (2010) 7927–7932.
[17] R.I. Morimoto, Proteotoxic stress and inducible chaperone networks in neurodegenerative disease and aging, Genes Dev. 22 (2008) 1427–1438.
[18] U. Nagaoka, K. Kim, N.R. Jana, H. Doi, M. Maruyama, K. Mitsui, F. Oyama, N. Nukina, Increased expression of p62 in expanded polyglutamine-expressing cells and its association with polyglutamine inclusions, J. Neurochem. 91 (2004) 57–68.
[19] C. Rothenberg, D. Srinivasan, L. Mah, S. Kaushik, C.M. Peterhoff, J. Ugolino, S. Fang, A.M. Cuervo, R.A. Nixon, M.J. Monteiro, Ubiquilin functions in autophagy and is degraded by chaperone-mediated autophagy, Hum. Mol. Genet. 19 (2010) 3219–3232.
[20] S.C. Shih, G. Prag, S.A. Francis, M.A. Sutanto, J.H. Hurley, L. Hicke, A ubiquitin-binding motif required for intramolecular monoubiquitylation, the CUE domain, EMBO J. 22 (2003) 1273–1281.
[21] M. Tanaka, Y. Machida, S. Niu, T. Ikeda, N.R. Jana, H. Doi, M. Kurosawa, M. Nekooki, N. Nukina, Trehalose alleviates polyglutamine-mediated pathology in a mouse model of Huntington disease, Nat. Med. 10 (2004) 148–154.

The American Journal of Pathology, Vol. 180, No. 4, April 2012

DOI: 10.1016/j.ajpath.2011.12.040

Molecular Pathogenesis of Genetic and Inherited Diseases

In Vivo Characterization of Mutant Myotilins

Etsuko Keduka,* Yukiko K. Hayashi,* Sherine Shalaby,* Hiroaki Mitsuhashi,*† Satoru Noguchi,* Ikuya Nonaka,* and Ichizo Nishino*

From the Department of Neuromuscular Research, National Institute of Neuroscience, National Center of Neurology and Psychiatry, Tokyo, Japan; and the Division of Genetics,† Children's Hospital Boston, Harvard Medical School, Boston, Massachusetts*

Myofibrillar myopathy (MFM) is a group of disorders that are pathologically defined by the disorganization of the myofibrillar alignment associated with the intracellular accumulation of Z-disk–associated proteins. MFM is caused by mutations in genes encoding Z-disk–associated proteins, including myotilin. Although a number of MFM mutations have been identified, it has been difficult to elucidate the precise roles of the mutant proteins. Here, we present a useful method for the characterization of mutant proteins associated with MFM. Expression of mutant myotilins in mouse tibialis anterior muscle by *in vivo* electroporation recapitulated both the pathological changes and the biochemical characteristics observed in patients with myotilinopathy. In mutant myotilin-expressing muscle fibers, myotilin aggregates and is costained with polyubiquitin, and Z-disk–associated proteins and myofibrillar disorganization were commonly seen. In addition, the expressed S60C mutant myotilin protein displayed marked detergent insolubility in electroporated mouse muscle, similar to that observed in human MFM muscle with the same mutation. Thus, *in vivo* electroporation can be a useful method for evaluating the pathogenicity of mutations identified in MFM. ***(Am J Pathol 2012, 180: 1570–1580; DOI: 10.1016/j.ajpath.2011.12.040)***

Myofibrillar myopathy (MFM) is a group of neuromuscular diseases with common morphological features such as disorganized myofibrillar alignment and accumulation of Z-disk–associated proteins.[1] Mutations in genes encoding Z-disk–associated proteins are known to cause MFM. Disease-associated mutations have been identified in six genes, including myotilin, desmin, αB-crystallin, ZASP, filamin C, and BAG3.[2,3] Elucidation of their pathogenicity, however, is sometimes difficult.

Myotilin (myofibrillar protein with titin-like immunoglobulin domains) is a 57-kDa protein with 10 exons encoded by the myotilin gene (*MYOT*) on chromosome 5q31. Myotilin consists of a unique serine-rich domain at the N-terminus and two Ig-like domains at the C-terminus.[4–7] Myotilin is highly expressed in skeletal and cardiac muscle, and localizes to the Z-disk,[4] which plays important roles in sarcomere assembly, actin filament stabilization, and muscle force transmission.[8,9] Myotilin interacts with several Z-disk–associated proteins, including α-actinin,[4] filamin C,[10,11] FATZ,[11] ZASP,[12] and MuRF ubiquitin ligase.[13] Myotilin also interacts with actin monomers and filaments through its Ig-like domains, which also mediate homodimerization.[14] Previous studies have shown that myotilin can bundle actin filaments *in vitro*, acting alone or in collaboration with α-actinin and filamin C.[4,14,15] Thus, myotilin is thought to play a role in anchoring and stabilizing actin filaments at the Z-disk, and is involved in the organization and maintenance of Z-disk integrity.[12] Missense mutations in *MYOT* have been associated with MFM,[16–18] limb girdle muscular dystrophy type 1A,[17,19,20] and distal myopathy.[21,22] We have previously identified a mutation p.Arg405Lys (R405K) in exon 9 in the second Ig-like domain of myotilin. The R405K mutant myotilin exhibited defective homodimerization and decreased interaction with α-actinin in a yeast 2-hybrid (Y2H) system.[23] All of the other previously reported *MYOT* mutations are located in exon 2 [14,16–18,24], with p.Ser60Cys (S60C) being one of the most common mutations. The pathogenic effects of *MYOT* mutations and

Supported by a Grant-in-Aid for Scientific Research from the Japan Society for the Promotion of Science; a Comprehensive Research on Disability Health and Welfare (20B-12, 20B-13) award from the Ministry of Health, Labor and Welfare; a Research on Intractable Diseases award from the Ministry of Health, Labor and Welfare; an Intramural Research Grant (23-4, 23-5, 23-6) for Neurological and Psychiatric Disorders, National Center of Neurology and Psychiatry; and a grant from the Japan Foundation for Neuroscience and Mental Health.

Accepted for publication December 29, 2011.

Supplemental material for this article can be found at *http://ajp.amjpathol.org* or at doi: 10.1016/j.ajpath.2011.12.040.

Address reprint requests to Yukiko K. Hayashi, M.D, Ph.D., Department of Neuromuscular Research, National Institute of Neuroscience, National Center of Neurology and Psychiatry, 4-1-1 Ogawahigashicho, Kodaira, Tokyo, 187-8502, Japan. E-mail: hayasi_y@ncnp.go.jp.

the disease mechanism involved remain poorly understood.

Model animals, such as transgenic mice, have contributed to understanding of the critical pathogenic events in MFM.[25–27] Some MFMs, including myotilinopathies, are late-onset and slowly progressive diseases.[1,3] To reproduce clinical and pathological features in model animals for such late-onset mild myopathy is both labor intensive and time consuming. Among the 10 missense mutations identified to date in patients with myotilinopathy,[14,16–18,23,24] only the Thr57Ile (T57I) mutation reproduces the pathological changes in transgenic mice after 12 months of age.[28] To screen for candidate mutations in MFM, a new method is required for demonstrating the pathogenicity of mutations. In the present study, we expressed mutant myotilin in mouse muscle by *in vivo* electroporation and were able to easily reproduce pathological changes similar to those observed in skeletal muscle from patients with *MYOT* mutations.

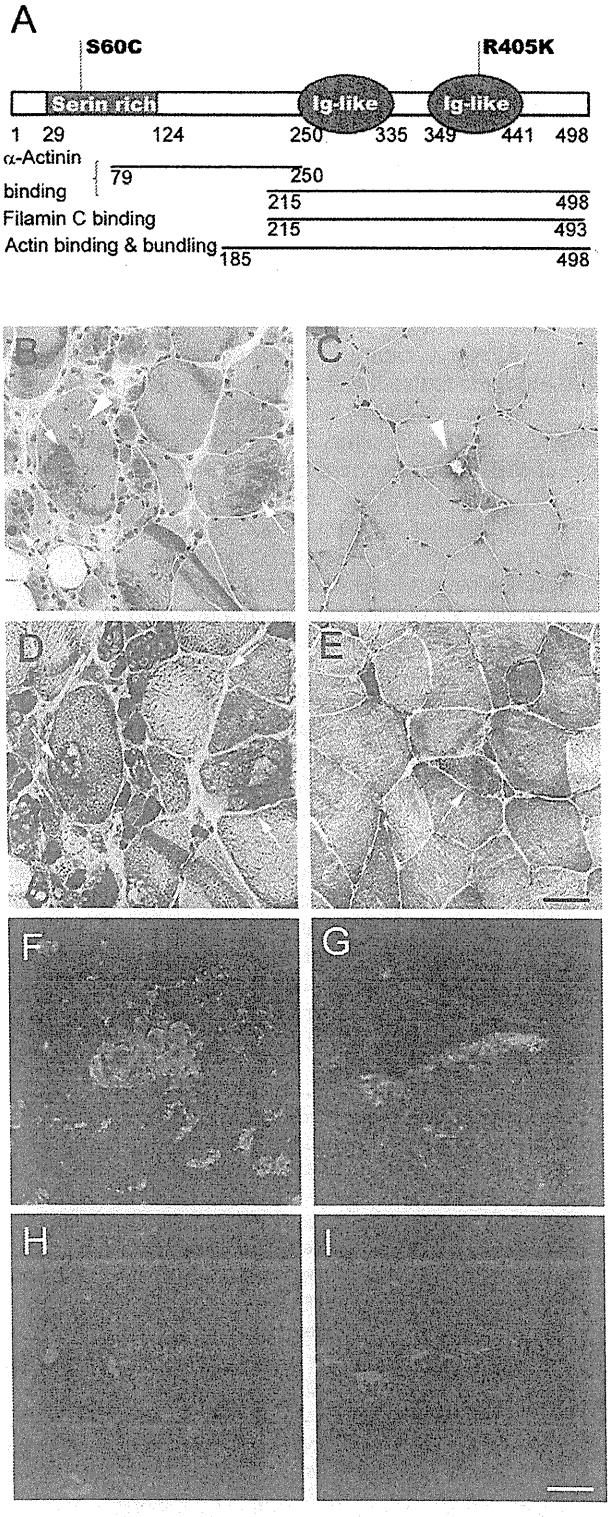

Materials and Methods

Clinical Materials

All clinical materials used in this study were obtained for diagnostic purposes with written informed consent. The studies were approved by the Ethical Committee of the National Center of Neurology and Psychiatry.

Genetic Analysis

Genomic DNA was isolated from peripheral lymphocytes or muscle specimens of patients, using standard techniques. Sequencing and mutation analysis of *MYOT* were performed as described previously.[23]

Plasmid Construction

We cloned full-length human myotilin cDNA and generated mutant myotilin (mMYOT) by site-directed mutagenesis, as described previously.[23] A C→G substitution at nucleotide position 179 and a G→A substitution at nucleotide 1214 were introduced to obtain p.S60C and p.R405K, respectively. A schematic of the location of these mutations in the structure of the myotilin protein is given in Figure 1A. For expression in mammalian cells, cDNAs of wild-type myotilin (wtMYOT) or mMYOT (S60C or R405K) were subcloned into pCMV-Myc vector (Ta-

Figure 1. Myotilin mutations and histopathological findings in myotilinopathy patients. **A:** Myotilin structure and disease-related mutations. p.Ser60Cys (S60C) is located in the serine-rich domain and p.Arg405Lys (R405K) is located in the second immunoglobulin (Ig)-like domain of myotilin. **B–I:** Pathological changes in muscles from patient 1 with *MYOT*S60C (**B**, **D**, **F**, and **H**) and from patient 2 with *MYOT*R405K (**C**, **E**, **G**, and **I**). **B:** Modified Gömöri trichrome (mGT) staining of biopsied skeletal muscle from patient 1 revealed markedly degenerated fibers with many spheroid protein inclusions (**arrows**). Some fibers had rimmed vacuoles (**arrowhead**). **C:** mGT staining of biopsied skeletal muscle from patient 2 revealed scattered fibers with rimmed vacuoles (**arrowhead**). **D:** NADH tetrazolium reductase (NADH-TR) staining of the serial section shown in **B** revealed markedly disorganized intermyofibrillar networks (**arrows**). **E:** NADH-TR staining of the serial section shown in **C** revealed disorganized intermyofibrillar networks (**arrow**). **F–I:** Coimmunostaining of muscles from patients using anti-myotilin (green) and anti-polyubiquitin (red) antibodies. **F:** Large accumulations of myotilin were observed in many fibers in patient 1. **G:** Small accumulations of myotilin were seen in some fibers in patient 2. Myotilin aggregates were positive for polyubiquitin in both patient 1 (**H**) and patient 2 (**I**). Scale bars: 50 μm (**B–E**); 20 μm (**F–I**).

kara Bio, Shiga, Japan). All constructs were verified by sequencing. Primer sequences are available on request.

Cell Culture, Transfection, and Immunocytochemical Analysis

C2C12 murine myoblast cells (American Type Culture Collection, Manassas, VA) were cultured in Dulbecco's modified Eagle's medium (Sigma-Aldrich, St. Louis, MO) supplemented with 10% fetal bovine serum (Invitrogen, Carlsbad, CA) at 37°C in a humidified atmosphere of 5% carbon dioxide. The cells were transiently transfected using FuGENE HD transfection reagent (Roche Diagnostics, Indianapolis, IN), according to the manufacturer's instructions. Forty-eight hours after transfection, the cells were fixed in 4% paraformaldehyde, permeabilized with 0.5% Triton-X 100, and costained with anti-Myc antibody (Sigma-Aldrich) and rhodamine-labeled phalloidin (Wako Pure Chemical Industries, Osaka, Japan) to detect transfected myotilin and actin filaments, respectively, according to standard protocol.[29]

In Vivo *Electroporation*

ICR mice were purchased from CLEA Japan (Fuji, Shizuoka, Japan). Animals were handled in accordance with the guidelines established by the Ethical Review Committee on the Care and Use of Rodents in the National Institute of Neuroscience, National Center of Neurology and Psychiatry. All mouse experiments were approved by the Committee. Five-week-old male ICR mice were anesthetized with diethyl ether, and the tibialis anterior (TA) muscles of mice were injected with 80 μg of purified Myc-tagged myotilin plasmid DNA. wtMYOT was injected to one side of TA muscle and mMYOT (S60C or R405K) was injected to the other side of TA muscle. *In vivo* transfection was performed using a square-wave electroporator (CUY-21SC; Nepa Gene, Ichikawa, Japan). A pair of electrode needles was inserted into the muscle to a depth of 3 mm to encompass the DNA injection sites. Each injected site was administered with three consecutive 50 ms-long pulses at the required voltage (50 to 90 V) to yield a current of 150 mA. After a 1-second interval, three consecutive pulses of the opposite polarity were administered. At 7 or 14 days after electroporation, mice were sacrificed by cervical dislocation, and TA muscles were isolated.

Histochemical and Immunohistochemical Analyses

Biopsied human muscles or electroporated mouse TA muscles were frozen in isopentane cooled in liquid nitrogen. Serial 10-μm cryosections were stained with modified Gömöri trichrome (mGT) and NADH-tetrazolium reductase (NADH-TR) and were subjected to a battery of histochemical methods. Immunohistochemistry was performed on serial 6-μm cryosections, as described previously.[29]

Antibodies

The primary antibodies used in this study were as follows: actin (Kantoukagaku, Tokyo, Japan), α-actinin (Sigma-Aldrich), BAG3 (Abcam, Tokyo, Japan), αB-crystallin (StressGen Biotechnologies, Victoria, BC, Canada), desmin (PROGEN Biotechnik, Heidelberg, Germany), filamin C (kindly provided by A.H. Beggs),[30] c-Myc (Sigma-Aldrich), c-Myc (PROGEN Biotechnik), myotilin (Proteintech Group, Chicago, IL), polyubiquitinated protein (Biomol International-Enzo Life Sciences, Plymouth Meeting, PA), GAPDH (Advanced ImmunoChemical, Long Beach, CA), and horseradish peroxidase-labeled anti-c-Myc antibody (Santa Cruz Biotechnology, Santa Cruz, CA).

Evaluation of Aggregates

Histochemical and immunohistochemical analyses were performed on cryosections of electroporated muscles sectioned at 500-μm intervals. The section containing the highest number of Myc-positive fibers (>100 fibers) was used. Myc-positive granules >1 μm in diameter were defined as aggregates. The Myc-positive fibers containing Myc-positive aggregates were counted among all Myc-positive fibers. Five mice each from the wtMYOT-, mMYOT S60C-, and mMYOT R405K-expressing groups were examined. To compare the number and size of Myc-positive aggregates per fiber, we measured the number and area of Myc-positive aggregates in 30 myofibers from each specimen using ImageJ software version 1.43 (NIH, Bethesda, MD). The results are presented as bar graphs (±SD) and histograms. Fifteen serial sections were immunoblotted to measure the amounts of electroporated Myc-tagged myotilin protein.

Electron Microscopy

For electron microscopy, cryosections (25 μm thick) of biopsied muscle with the S60C mutation (patient 1) were fixed with 2% glutaraldehyde in 100 mmol/L cacodylate buffer for 15 minutes on ice. After a shaking with a mixture of 4% osmium tetroxide, 1.5% lanthanum nitrate, and 200 mmol/L s-collidine for 1 to 2 hours, samples were embedded in epoxy resin. TA muscles of 5-week-old ICR mice were coelectroporated with pEGFP-C1 plasmid (Clontech, Tokyo, Japan), which encodes enhanced green fluorescent protein (EGFP), and with either Myc-wtMYOT or Myc-mMYOT (S60C or R405K) plasmid (40 μg each). As a control, pEGFP-C1 plasmid was electroporated alone. TA muscles were isolated 7 and 14 days after electroporation. EGFP-positive regions were trimmed under a fluorescence microscope and fixed with 2% glutaraldehyde in 100 mmol/L cacodylate buffer for 3 hours. After a shaking with a mixture of 4% osmium tetroxide, 1.5% lanthanum nitrate, and 200 mmol/L s-collidine for 2 to 3 hours, samples were embedded in epoxy resin. Semithin sections (1 μm thick) were stained with Toluidine Blue. Ultrathin sections (100 nm thick) were stained with uranyl acetate and lead citrate, and were analyzed at 120 kV using a Tecnai Spirit transmission electron microscope (FEI, Hillsboro, OR).